arXiv:1807.02897v2 [hep-ph] 4 Sep 2018

Odderon and proton substructure from a model-independent Lévy imaging of elastic pp and $p\bar{p}$ collisions

T. Csörgő,[a,b] **R. Pasechnik,**[c,d] **A. Ster**[a]

[a] *MTA WIGNER FK, H-1525 Budapest 114, POB 49, Hungary*
[b] *EKU KRC, H-3200 Gyöngyös, Mátrai út 36, Hungary*
[c] *Department of Astronomy and Theoretical Physics, Lund University, SE-223 62 Lund, Sweden*
[d] *Nuclear Physics Institute ASCR, 25068 Řež, Czech Republic*

E-mail: tcsorgo@cern.ch, roman.pasechnik@thep.lu.se

Abstract: We describe a new and model-independent Lévy imaging method, and reconstruct the forward scattering amplitude for high-energy pp and $p\bar{p}$ elastic scattering, with quality fits to the published data sets. This method allows us to determine the excitation function of the shadow profile $P(b)$, the elastic slope $B(t)$ and the nuclear phase $\phi(t)$ functions of pp and $p\bar{p}$ collisions directly from the data. Surprisingly, notable qualitative differences in $B(t)$ for pp and for $p\bar{p}$ collisions point towards an Odderon effect. As a by-product, we clearly identify the proton substructure with two different sizes at the ISR and LHC energies, that has striking similarity to a dressed quark (at the ISR) and a dressed diquark (at the LHC). We present model-independent results for the corresponding sizes and cross-sections for such a substructure for the existing data at different energies.

Keywords: Elastic proton-proton and proton-antiproton scattering, diffraction, nucleon imaging

Contents

1 Introduction **2**

2 Model-independent Lévy analysis of elastic pp and $p\bar{p}$ scattering **3**
- 2.1 Differential, total and elastic cross-sections 8
- 2.2 Four-momentum transfer dependent elastic slope $B(t)$ 10
- 2.3 Shadow profile functions 13

3 Data analysis **14**
- 3.1 Looking for Odderon effects 16
- 3.2 Excitation function of the shadow profiles 17
- 3.3 Results for the nuclear slope parameter 18
- 3.4 Evidence for proton substructure 24
- 3.5 Results for $\rho(t)$ 25
- 3.6 Results for the nuclear phase $\phi(t)$ 26

4 Discussion **27**
- 4.1 Qualitative features 28
- 4.2 Highlighted results 29

5 Summary and conclusions **32**

A Lévy expansion fits to elastic pp collisions: full acceptance region **34**

B Lévy expansion fits to elastic $p\bar{p}$ collisions: full acceptance region **36**

C Lévy fits to elastic pp collisions at large $|t|$ **37**

D Lévy fits to elastic pp collisions at small $|t|$ **39**

"What we pay attention to is largely determined by our expectations of what should be present."

Christopher Chabris

1 Introduction

The TOTEM Collaboration at the Large Hadron Collider (LHC) at CERN has released recently two new data sets about the first measurements of the total, elastic and differential cross sections, as well as the ρ-parameter, of elastic pp collisions at the currently highest available energy of $\sqrt{s} = 13$ TeV [1, 2]. Taken together, these papers indicate the influence of an odd-under-crossing (or C-odd) contribution to the forward scattering amplitude, traditionally called the Odderon [3], or in more modern language of Quantum Chromo Dynamics (QCD), an odd-gluon (predominantly three-gluon) bound state, a quarkless excitation sometimes also referred to as a vector glueball. As far as we know, the properties like the $\sqrt{s}$ and t dependences of the differential cross-section of an Odderon contribution at the LHC energies were determined from pp and $p\bar{p}$ collisions first in Ref. [4].

The new TOTEM preliminary results [1, 2] generated a burst of high-level and vigorous theoretical debate about the correct interpretation of these data, see Refs. [5]–[18]. All possible extreme views were present among these papers, including claims for a maximal Odderon effect [14] and claims of lack of any significant Odderon effects, see Refs. [10, 18].

In this paper, we investigate earlier, published data and a recently released, new TOTEM preliminary data set [19], to look for the Odderon effects in elastic pp collisions, and for the interpretation of the data, using a new and model-independent imaging technique, the Lévy series. Our analysis is based on the TOTEM preliminary data as presented by F. Nemes for the TOTEM Collaboration in Ref. [19].

We find that clear, but indirect signals of Odderon effects are present in the differential cross-section of elastic pp and $p\bar{p}$ scattering, as indicated by the difference of the four-momentum transfer dependence of the elastic slope $B(t)$ for pp and for $p\bar{p}$ collisions. A less evident but clear difference is also identified between the nuclear phase $\phi(t)$ of pp and $p\bar{p}$ collisions in the TeV energy range.

Although our analysis was motivated by the search for Odderon effects, our most surprising result is that we find a clear-cut evidence for a proton substructure having two distinct sizes in the GeV and TeV energy ranges, respectively. We estimate these sizes and the corresponding contributions to the total pp cross-section at the ISR and Tevatron/LHC energies.

The structure of the presentation is as follows. In Section 2, we present the model-independent imaging approach of Lévy expansions, in Section 3, we apply this method in a comprehensive analysis of elastic pp and $p\bar{p}$ collisions, and in Section 4, we discuss and interpret the results, as well as present the indirect signals of Odderon effects in elastic scattering in the TeV energy range. Finally, we summarize and conclude in Section 5.

This manuscript is closed by four Appendices. Appendix A details the results of the Lévy expansion fits to elastic pp scattering data for the whole available region of t. Appendix B

shows the individual fits to elastic $p\bar{p}$ scattering data. Appendix C describes fits to the tails (i.e. in the large-$|t|$ region just after the dip and the bump structure) of the differential cross-section of elastic pp scattering for all the experimentally accessed energies. These fits indicate an evidence for a proton substructure. Appendix D details Lévy fits to the cone (small-$|t|$) regions of elastic pp scattering, indicating that the proton size grows self-similarly in the GeV energy range, but at the LHC energies of $\sqrt{s} = 7$ and 13 TeV, something drastically changes, such that the protons keep on growing but their shape is also becomes significantly different from their shape in the ISR energy range of $\sqrt{s} = 23.5$ – 62.5 GeV.

2 Model-independent Lévy analysis of elastic pp and $p\bar{p}$ scattering

We describe a model-independent Lévy series, that is a generalization of the Laguerre, Edgeworth [20] and Lévy expansion [21] methods proposed to analyze nearly Lévy stable source distributions in the field of particle correlations and femtoscopy. The key point of this method is to have a look at the data, guess their approximate shape (for example, Gaussian, exponential or Lévy-stable shape) and then develop a systematic method to characterize the deviations from the approximate shape with the help of a dimensionless variable denoted in this paper by z, and a complete orthonormal set of polynomials that are orthogonal with respect to the assumed zeroth order shape or weight function $w(z)$. We recommend Ref. [20] for detailed discussions and for the convergence criteria of such expansions given in general terms. This way one may find the minimal number of necessary expansion coefficients.

For example, if the data follow the guessed approximate shape precisely, that can be clearly demonstrated by fitting the series to the data and finding that all the expansion coefficients that measure deviations from the zeroth-order shape are within errors consistent with zero. Indeed, the PHENIX Collaboration analyzed recently Bose-Einstein correlations of $\sqrt{s_{NN}} = 200$ GeV Au+Au collisions [22], and found that they are well described by the Lévy stable source distributions. The accuracy of the Lévy description was tested by a Lévy expansion of the Bose-Einstein correlation functions, as proposed in Ref. [23], to find that the first-order deviations from the Lévy stable source distributions within errors are consistent with zero [22].

The data analysis method of Ref. [23] was developed first for the functions that may oscillate between positive and negative values. However, the differential cross-section of elastic scattering is measured as an angular-dependent hit distribution, so it is a positive definite function, related to the modulus square of the forward scattering amplitude. Hence, we describe this expansion at the amplitude level, with complex expansion coefficients, and then take the modulus square of such an amplitude to get a positive-definite form.

The differential cross-section of elastic scattering at high energies is measured as a function of the four-momentum transfer squared, the Mandelstam variable $t = (p_1 - p_3)^2 < 0$. A differential cross-section of elastic scattering starts at the optical point at $t = 0$, decreases quickly and nearly exponentially in $|t|$, as typically characterized by an exponential slope parameter B, as follows: $\frac{d\sigma}{dt} = A \exp(-B|t|)$. The region, where such a behaviour is approxi-

mately valid, is called a diffractive cone, and such a featureless exponential decay corresponds to a nearly Gaussian distribution of the centers of elastic scattering [24]. This region is followed by (one or more) alternating diffractive minima and maxima, finally at high four-momentum transfers, a diffractive tail might be seen as well. For more details and for an introduction and review of diffraction before the start of the LHC measurements, see Ref. [24].

We know from the TOTEM analysis of $\sqrt{s} = 8$ TeV elastic pp scattering data, that the differential cross-section in the diffraction cone, at $|t|$ values below the diffraction minimum, deviates significantly from an exponential shape [25]. This deviation is a subtle, but it is more than a 7σ effect [25]. Using this knowledge, we assume that the forward scattering amplitude is nearly (but not completely) exponential in $|t|$, i.e. we assume that it is approximately described by a (Fourier-transformed) Lévy stable source distribution: $d\sigma/dt \propto \exp\left(-(R^2|t|)^\alpha\right)$. The conventional exponential behaviour corresponds to the $\alpha = 1$ special case. This way the deviation from the exponential behaviour can be quantified by a single parameter. If the value of the exponent α is significantly different from unity, it evidences a non-exponential behaviour of the differential cross-section of elastic scattering. Later on, we shall see that this is a very fortunate approach, and it connects the imaging of the differential cross-sections of high-energy pp and $p\bar{p}$ collisions with the Lévy stable source distributions that are ubiquitous in Nature [26].

We also know that the differential cross-section of high-energy pp and $p\bar{p}$ collisions has a diffractive minimum, followed by a second maximum, that is followed by an extended tail. Thus, the behaviour of the differential cross-sections at large $|t|$ has structures that deviate from a simple Lévy stable source. In this paper, we attempt to characterize these structures with an orthonormalized Lévy expansion. This way we obtain a new imaging method, that we describe in detail below, and apply it to reconstruct the shadow profile functions, the t-dependent slope parameters and the t-dependent nuclear phases in high-energy pp as well as $p\bar{p}$ collisions.

These physical and mathematical assumptions result in the following formulae for the differential cross-section of elastic pp and $p\bar{p}$ collisions:

$$\frac{d\sigma}{dt} = A\, w(z|\alpha) \left| 1 + \sum_{j=1}^{\infty} c_j l_j(z|\alpha) \right|^2 , \tag{2.1}$$

$$w(z|\alpha) = \exp(-z^\alpha) , \tag{2.2}$$

$$z = |t|R^2 \geq 0 , \tag{2.3}$$

$$c_j = a_j + ib_j , \tag{2.4}$$

where $w(z|\alpha)$ is the Lévy weight function, and a dimensionless variable z is introduced as the magnitude of the four-momentum transfer squared $|t|$ multiplied by a Lévy scale parameter R squared, where R is measured in units of fm (natural units $c = \hbar = 1$ are adopted here and below). Note that the $w(z|\alpha)$ is also called the stretched exponential distribution, which, for $\alpha = 1$ limiting case, corresponds to the exponential distribution. This shape actually

corresponds to a Fourier-transformed and modulus squared symmetric Lévy-stable source distribution centered on zero. The orthonormal set of Lévy polynomials, defined below, are denoted as $l_j(z|\alpha)$. The complex expansion coefficients are c_j, with a_j and b_j standing for the real and the imaginary parts of c_j, respectively.

In the forthcoming, we shall refer to the zeroth-order ($c_i = 0$) Lévy expansion simply as a Lévy fit. Let us clarify here that these so-called Lévy fits actually correspond to the Fourier-transformed and modulus squared, symmetric Lévy stable source distributions, as approximations to the shape of the forward scattering amplitude of elastic pp scattering, $t_{el}(b)$. This elastic amplitude will be introduced and detailed in Subsection 2.1. For more details on the application of Lévy stable source distributions in particle correlations and femtoscopic measurements, we recommend Refs. [20, 27, 28].

The expansion (2.1) is expected to converge to nearly Lévy shaped data, if the order of the series n is chosen to be sufficiently large, i.e. $n \to \infty$. In practice, however, third-order ($n = 3$) Lévy series already converged to the data measured at $\sqrt{s} < 1$ TeV, with confidence levels (i.e. the probability that the Lévy series or expansion of the forward scattering amplitude converges to the differential cross-section under investigation) corresponding to a statistically acceptable description. In order to gain a statistically marginal or acceptable description of the high precision TOTEM data at 7 TeV and preliminary data at 13 TeV, we had to go to the fourth-order Lévy series, $n = 4$, in these two cases. For reasons of consistency, and in order to eliminate fitting artefacts that may show up if one compares different orders of the Lévy expansions with one another, we decided to re-fit all the pp elastic scattering data with the fourth-order Lévy expansion and to show only these results. However, when applying a similar procedure to $p\bar{p}$ elastic scattering, it turned out that the range of the data around the dip position was too limited in this case, and the fourth-order Lévy expansion terms could not be determined in a reliable and reasonable manner. So we decided to show only the fit results of the third-order Lévy expansions for the $p\bar{p}$ elastic scattering data.

As we explicitly demonstrate in Appendices C and D, in certain limited intervals of $|t|$, Lévy fits without correction terms (i.e. for $c_i = 0$, $i \geq 1$) provided statistically not unacceptable, but in contrast, rather good quality fits and the corresponding confidence levels. These results suggest that the Lévy series is a reasonable representation of the forward scattering amplitude of elastic pp and $p\bar{p}$ collisions.

The first four orthogonal (but not yet normalized) Lévy polynomials denoted as $L_i(z\,|\,\alpha)$

are found as follows

$$L_0(z\,|\,\alpha) = 1, \tag{2.5}$$

$$L_1(z\,|\,\alpha) = \det\begin{pmatrix} \mu_{0,\alpha} & \mu_{1,\alpha} \\ 1 & z \end{pmatrix}, \tag{2.6}$$

$$L_2(z\,|\,\alpha) = \det\begin{pmatrix} \mu_{0,\alpha} & \mu_{1,\alpha} & \mu_{2,\alpha} \\ \mu_{1,\alpha} & \mu_{2,\alpha} & \mu_{3,\alpha} \\ 1 & z & z^2 \end{pmatrix}, \tag{2.7}$$

$$L_3(z\,|\,\alpha) = \det\begin{pmatrix} \mu_{0,\alpha} & \mu_{1,\alpha} & \mu_{2,\alpha} & \mu_{3,\alpha} \\ \mu_{1,\alpha} & \mu_{2,\alpha} & \mu_{3,\alpha} & \mu_{4,\alpha} \\ \mu_{2,\alpha} & \mu_{3,\alpha} & \mu_{4,\alpha} & \mu_{5,\alpha} \\ 1 & z & z^2 & z^3 \end{pmatrix}, \qquad \ldots \quad \text{etc}\,, \tag{2.8}$$

where

$$\mu_{n,\alpha} = \int_0^\infty dz\; z^n \exp(-z^\alpha) = \frac{1}{\alpha}\,\Gamma\left(\frac{n+1}{\alpha}\right)$$

and Euler's gamma function is defined as

$$\Gamma(x) = \int_0^\infty dz\; z^{x-1} e^{-z}. \tag{2.9}$$

The normalization of these Lévy polynomials is straightforwardly expressed as follows:

$$l_j(z\,|\,\alpha) = D_j^{-\frac{1}{2}} D_{j+1}^{-\frac{1}{2}} L_j(z\,|\,\alpha), \qquad \text{for} \quad j \geq 0\,, \tag{2.10}$$

where $D_0 = 1$ and, in general, $D_j \equiv D_j(\alpha)$ stands for the Gram-determinant of order j, defined as

$$D_0(\alpha) = 1, \tag{2.11}$$

$$D_1(\alpha) = \mu_{0,\alpha}, \tag{2.12}$$

$$D_2(\alpha) = \det\begin{pmatrix} \mu_{0,\alpha} & \mu_{1,\alpha} \\ \mu_{1,\alpha} & \mu_{2,\alpha} \end{pmatrix}, \tag{2.13}$$

$$D_3(\alpha) = \det\begin{pmatrix} \mu_{0,\alpha} & \mu_{1,\alpha} & \mu_{2,\alpha} \\ \mu_{1,\alpha} & \mu_{2,\alpha} & \mu_{3,\alpha} \\ \mu_{2,\alpha} & \mu_{3,\alpha} & \mu_{4,\alpha} \end{pmatrix}, \tag{2.14}$$

$$D_4(\alpha) = \det\begin{pmatrix} \mu_{0,\alpha} & \mu_{1,\alpha} & \mu_{2,\alpha} & \mu_{3,\alpha} \\ \mu_{1,\alpha} & \mu_{2,\alpha} & \mu_{3,\alpha} & \mu_{4,\alpha} \\ \mu_{2,\alpha} & \mu_{3,\alpha} & \mu_{4,\alpha} & \mu_{5,\alpha} \\ \mu_{3,\alpha} & \mu_{4,\alpha} & \mu_{5,\alpha} & \mu_{6,\alpha} \end{pmatrix}, \qquad \ldots \quad \text{etc.} \tag{2.15}$$

These normalized Lévy polynomials $l_j(z|\alpha)$ are, as far as we know, newly introduced in this work, while the unnormalized Lévy polynomials $L_j(z|\alpha)$ were introduced earlier in Ref. [21].

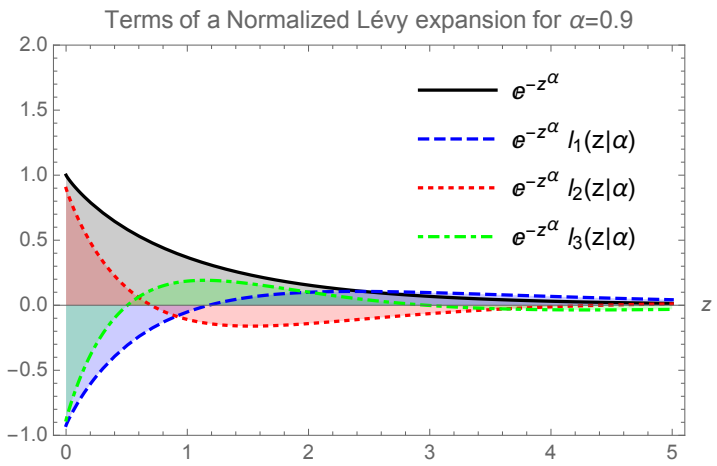


Figure 1. Illustration of the first three Lévy polynomials for $\alpha = 0.9$.

The orthonormality of $\{l_j(z|\alpha)\}_{j=0}^{\infty}$ with respect to a Lévy or stretched exponential weight is expressed by the following relation:

$$\int_0^{\infty} dz \exp(-z^{\alpha}) l_n(z\,|\,\alpha) l_m(z\,|\,\alpha) = \delta_{n,m}\,. \tag{2.16}$$

The first few of these orthonormal Lévy polynomials are illustrated in Fig. 1 for a specific value of $\alpha = 0.9$. More details of them, in particular the $\alpha = 2$ Gaussian, the $\alpha = 1$ Laguerre special cases and their explicit forms are being described in Refs. [29, 30].

Once we have a statistically acceptable description of the differential cross-section of elastic pp and $p\bar{p}$ collisions, we can build the forward scattering amplitude with the help of the Lévy imaging method, and we can then compare the resulting shadow profiles of pp and $p\bar{p}$ collisions without any model-dependent assumptions. Similarly, we can extract the t-dependence of the nuclear slope $B(t)$ directly from the data, as well as compare its behaviour for pp collisions with that of $p\bar{p}$ collisions. The same is true for the nuclear phase and for the t-dependent ρ-parameter as well.

In fact, in our analysis we rely only on the convergence of the Lévy series (or Lévy expansion), that we have tested by the usual χ^2-optimization methods with the CERN Minuit package and by evaluating the confidence level.

Based on our experience with extracting $B(t)$, $\rho(t)$ and the shadow profile $P(b)$ from pp and $p\bar{p}$ elastic collision data, we can definitely state that the precise reproduction of the measured data points, with a statistically acceptable confidence level of CL $> 0.1\%$ is a necessary condition for interpreting our fit results. We have achieved such good quality fits in each case of the analysis of the published, final data, except for the 7 TeV pp elastic scattering data, where we reached a marginal confidence level of CL $= 0.002\%$, as indicated in Fig. 2. After scrutinizing this fit, presented in Fig. 2, we decided to interpret the parameters of this fit as well. But in principle, in order to get the final errors of our parameters, we may

need to repeat the analysis by taking into account the full covariance matrix. In case of the TOTEM preliminary 13 TeV data set, we also warn the reader that these data points and their errors are still in a preliminary phase, so we have determined the best preliminary values of the parameters of the Lévy series from the minimum of the χ^2-distribution. Also, we have estimated the error on them so that the estimated preliminary value of the confidence level of these fits CL$'$ satisfies the criteria for good quality fits, i.e. 99.9% > CL$'$ > 0.1 %. The preliminary value of the confidence level of fits to the TOTEM preliminary data at $\sqrt{s} = 13$ TeV indeed satisfies these criteria, CL$'$ = 96%, as indicated in Fig. 3.

Fig. 6 represents the summary plot of the Lévy fits, $d\sigma/dt = A\exp(-(R^2|t|)^\alpha)$, that correspond to the zeroth-order of the Lévy expansion detailed in this manuscript, to the *tails* of the elastic *pp* scattering data at ISR and LHC energies from $\sqrt{s} = 23.4$ GeV up to 13 TeV, with $\alpha = 0.9$ fixed. These results are detailed in Appendix C, and are explained in terms of the newly identified proton substructure in Subsection 3.4. Namely, rather clearly, a smaller substructure is seen in the ISR energy range, that is invariant for the (relatively small) change of $\sqrt{s}$, as evidenced by the dashed lines that (except an overall normalization factor) follow the same curves. It is apparent from the visualization of Fig. 6, that at $\sqrt{s} = 7$ and 13 TeV, the slope of these dashed lines changes dramatically: a proton substructure of a different size is found that is apparently (within the errors) the same both at 7 and at 13 TeV.

Fig. 7 represents a summary plot of the Lévy fits, $d\sigma/dt = A\exp(-(R^2|t|)^\alpha)$ to the *cone* or low-$|t|$ part of the elastic *pp* scattering data at ISR and LHC energies from $\sqrt{s} = 23.4$ GeV up to 13 TeV, with $\alpha = 0.9$ fixed. These results are detailed in Appendix D. The gradual steepening of the slope of the fitted curves indicate, that the Lévy scale R, characterizing the overall size of the proton, was increasing monotonically with increasing energy $\sqrt{s}$. This behaviour can be explained in terms of the proton size growing self-similarly in the ISR energy range, as evident also from the excitation function of the shadow-profiles at $23.5 \leq \sqrt{s} \leq 62.5$ GeV. This effect is discussed and detailed in Subsection 3.2. However, at $\sqrt{s} = 7$ and 13 TeV, the $\alpha = 0.9$ fixed fits failed, indicating that not only the size of the proton increases with an increase of collision energies, but also the shape of the protons changes. These results can be explained in terms of the evolving shape of the shadow profiles at 7 and 13 TeV, as described in Subsection 3.2, due to a saturation of the shadow profile functions $P(b) \approx 1$ in the $b \leq 0.4 - 0.5$ fm region at 7 and 13 TeV, respectively.

2.1 Differential, total and elastic cross-sections

The conventional form of the elastic differential cross section

$$\frac{d\sigma}{dt} = \frac{1}{4\pi}|T_{el}(\Delta)|^2\,, \qquad \Delta = \sqrt{|t|}\,, \tag{2.17}$$

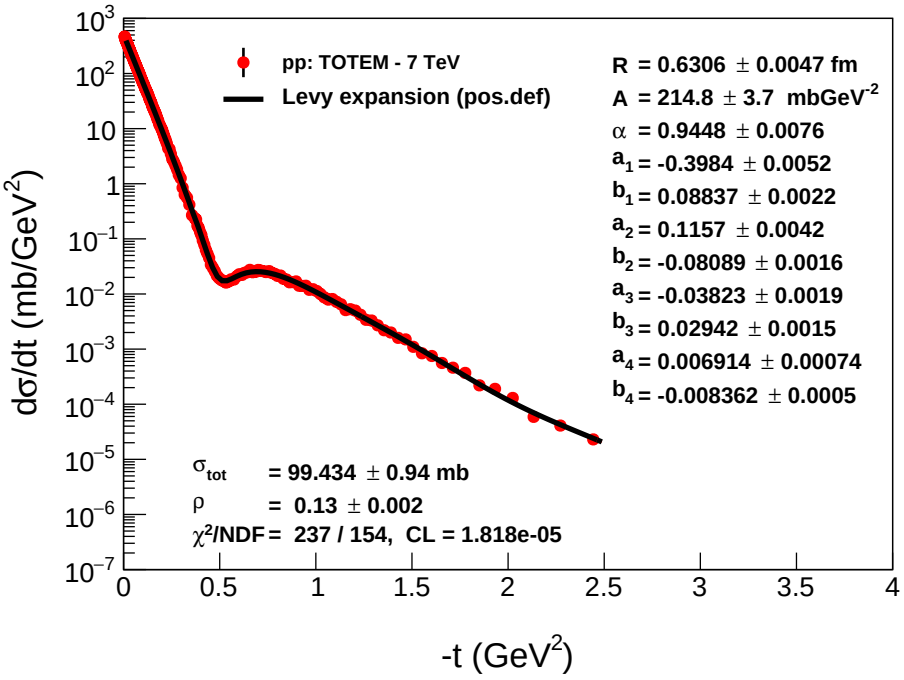


Figure 2. Model-independent Lévy expansion results from fits to elastic *pp* scattering data by the TOTEM Collaboration at the LHC energy of $\sqrt{s} = 7$ TeV. Although the fit quality is marginal, CL = 0.002%, the fitted curve follows the data so closely that we decided to interpret the fit parameters, noting that the errors on the best values of the parameters are likely underestimated.

provides us with the key expression for the complex-valued forward scattering amplitude $T_{el}(\Delta)$ in terms of a Lévy series

$$T_{el}(\Delta) = i\sqrt{4\pi A}\,\exp\left(-\frac{1}{2}z^{\alpha}\right)\left[1+\sum_{i=1}^{\infty}c_i l_i(z|\alpha)\right], \tag{2.18}$$

$$z = \Delta^2 R^2 = |t|R^2\,. \tag{2.19}$$

Then, according to the optical theorem, the total cross section is found as

$$\sigma_{\rm tot} \equiv 2\,{\rm Im}\,T_{el}(\Delta=0) = 2\,\sqrt{4\pi A}\,\left(1+\sum_{i=1}^{\infty}a_i l_i(0|\alpha)\right), \tag{2.20}$$

while the ratio of the real to imaginary parts of the elastic amplitude

$$\rho(t) \equiv \frac{{\rm Re}\,T_{el}(\Delta)}{{\rm Im}\,T_{el}(\Delta)} = -\left.\frac{\sum_{i=1}^{\infty}b_i l_i(z|\alpha)}{1+\sum_{i=1}^{\infty}a_i l_i(z|\alpha)}\right|_{z=tR^2} \tag{2.21}$$

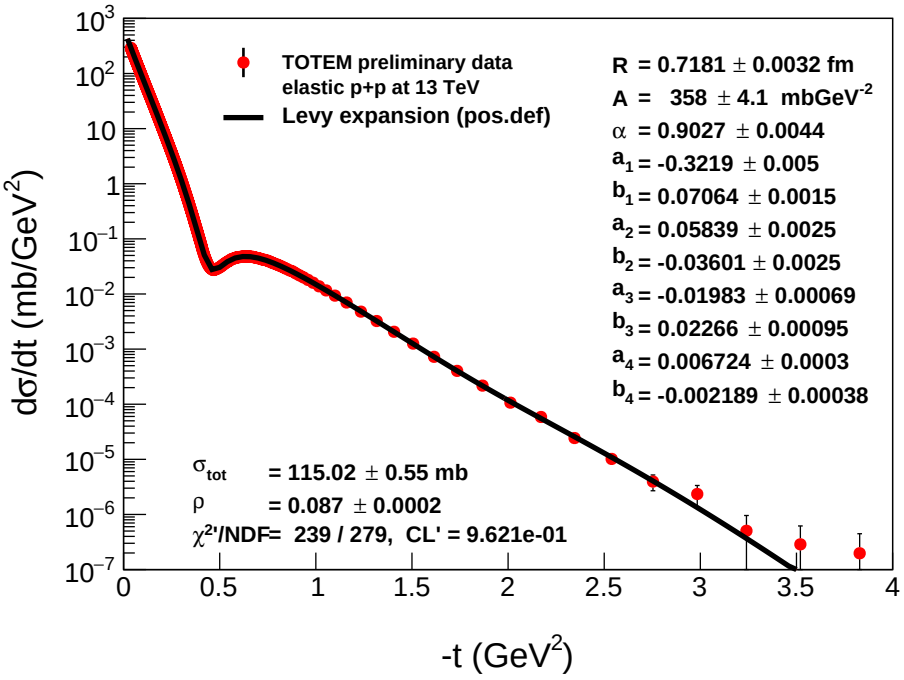


Figure 3. Model-independent Lévy expansion results from fits to the TOTEM preliminary elastic pp scattering data at the currently largest LHC energy of $\sqrt{s} = 13$ TeV. The errors on the fit parameters and the fit quality are also preliminary, as indicated by a prime ($\prime$) on the measures of the fit quality, the $\chi^{2\prime}$ and the confidence level CL$' = 96\%$.

is known as the ρ-parameter, in consistency with the traditional form of the forward elastic differential cross section

$$\frac{d\sigma}{dt}\Big|_{t\to 0} = \frac{(1+\rho_0^2)\sigma_{\rm tot}^2}{16\pi}\,, \qquad \rho_0 = \rho(t=0)\,. \tag{2.22}$$

It is also interesting to evaluate the total elastic cross-section, σ_{el}. In this calculation, we utilize the orthonormality of the Lévy polynomials $l_n(z|\alpha)$ to obtain

$$\sigma_{el} = \int_0^\infty d|t|\frac{d\sigma}{dt} = \frac{A}{R^2}\left[\frac{1}{\alpha}\Gamma\left(\frac{1}{\alpha}\right) + \sum_{i=1}^{\infty}(a_i^2+b_i^2)\right]\,. \tag{2.23}$$

2.2 Four-momentum transfer dependent elastic slope $B(t)$

The t-dependent elastic slope $B(t)$ is traditionally defined as

$$B(t) \equiv \frac{d}{dt}\left(\ln\frac{d\sigma}{dt}\right)\,. \tag{2.24}$$

There is a great current interest in the value of this function at $t = 0$ at LHC energies. Traditionally, the elastic slope is determined as $B = B(t=0)$. Let us note that this requires an

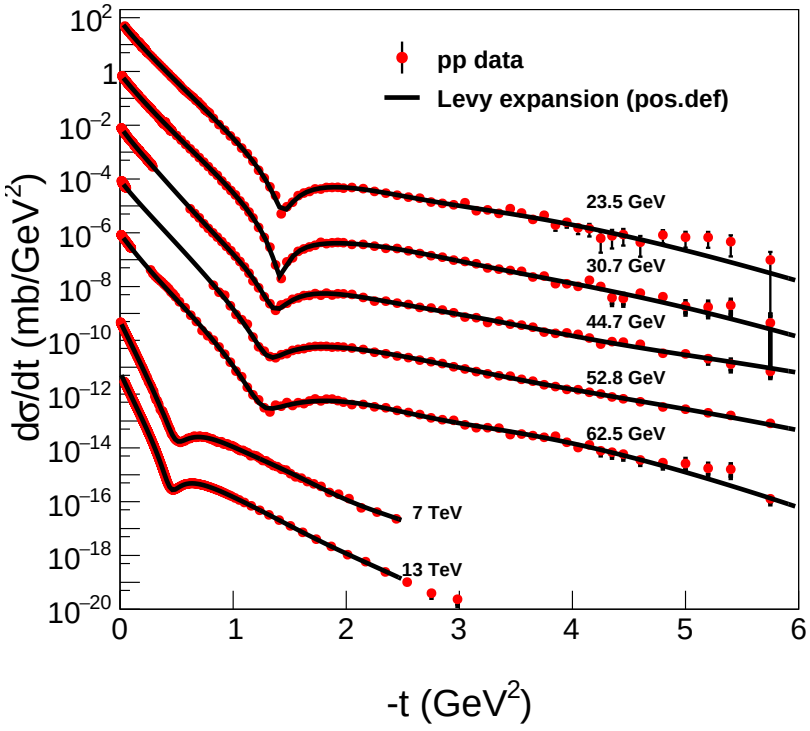


Figure 4. Summary plot of the model-independent, fourth-order Lévy expansion fits to the elastic pp scattering data at ISR and LHC energies ranging from from $\sqrt{s} = 23.4$ GeV up to 7 TeV. These fits are detailed in Appendix A.

extrapolation of the measured differential cross-sections to the $t = 0$ optical point. Frequently, an exponential approximation is applied, however, at the very low-$|t|$ region the Coulomb-Nuclear interference complicates such an extrapolation as well [25].

At this point, it is important to emphasize, that the Lévy series utilized in this paper to represent the forward scattering amplitude is not an analytic function at $t = 0$ if $\alpha < 1$, hence formally our expressions for B may not exist, as $B(t)$ is well-defined only for $|t| > 0$ in this case. However, if $\alpha = 1$, the cone region decreases exponentially and the forward scattering amplitude becomes an analytic function at $t = 0$. Hence, it is very important to determine the value of α precisely from the analysis of the elastic differential cross-section data.

Note that B is related to the root-mean-square (RMS) radius of the impact-parameter b-dependent elastic amplitude $t_{el}(b)$. It is well known that for Lévy-stable source distributions, that are our zeroth-order choices for the impact parameter dependent elastic amplitudes, the RMS of the source is divergent, if the Lévy index of stability $\alpha_L < 2$ [27], with the exception of the Gaussian case, corresponding to $\alpha_L = 2$, when the RMS of the source is finite. Due to the importance of this point, we have dedicated Appendix D to investigate if such a non-analytic

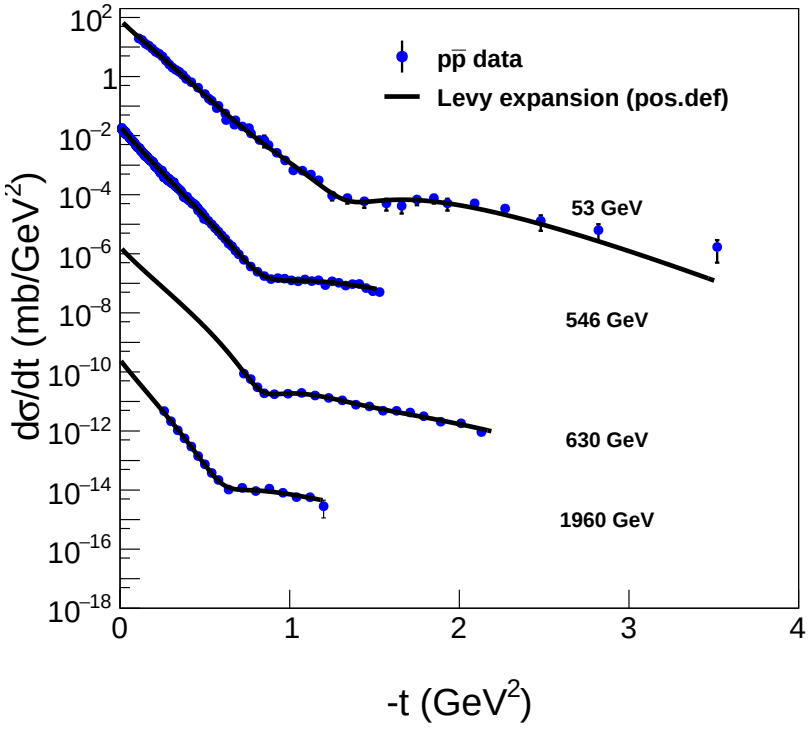


Figure 5. Summary plot of the model-independent, third-order Lévy expansion fits to the elastic $p\bar{p}$ scattering data at ISR, S$p\bar{p}$S, and Tevatron energies ranging from $\sqrt{s} = 23.4$ GeV up to 1.96 TeV. The fits converged, error matrix was accurate and CL ≥ 0.1 % for these fits, that were obtained with $\alpha = 0.9$ and $R = 0.65$ fm (both values are fixed). These fits are detailed in Appendix B.

model at $t = 0$ as the Lévy-stable source distribution of $t_{el}(b)$ can describe reasonably well the pp elastic differential cross-section data. Actually, we find that this is indeed a very good approximation to the data in the ISR energy range of $23.5 \leq \sqrt{s} \leq 62.5$ GeV, as explicitly demonstrated with $\alpha = 0.9$ fixed fits in Appendix D. Let us note here that the cone region of TOTEM data at $\sqrt{s} = 7$ and 13 TeV can also be well described in the same cone (or low-$|t|$) region, if the parameter α is released, corresponding to a change of the proton shape in the TeV energy range.

For more detailed examples and for the introduction of Lévy stable source distributions to femtoscopy in high-energy particle and nuclear physics, with an emphasis at their non-analytic nature of their Fourier-transform, we recommend Ref. [31].

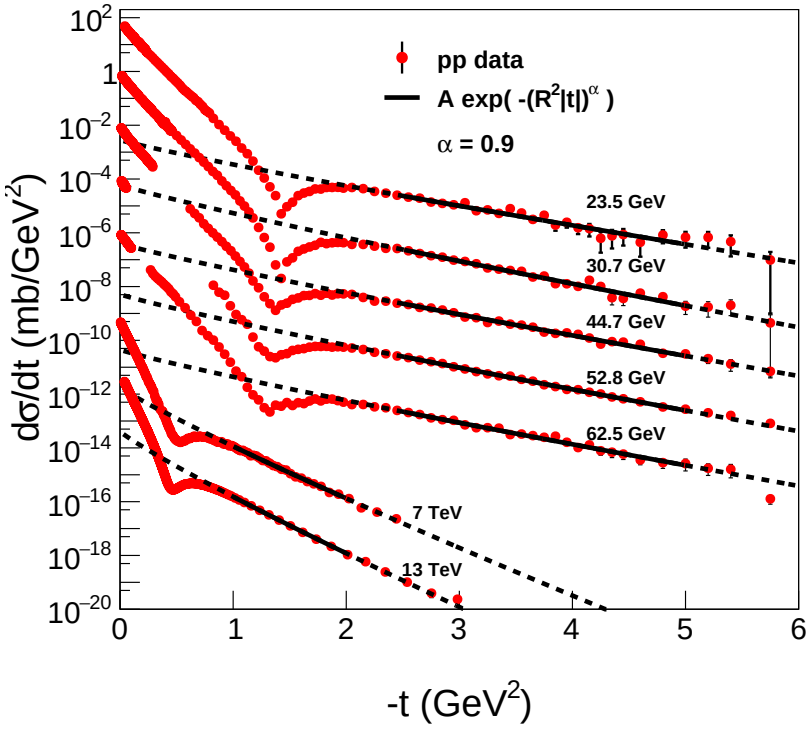


Figure 6. Summary plot of the Lévy fits, $d\sigma/dt = A\exp(-(R^2|t|)^\alpha)$ to the tails of the elastic pp scattering data at ISR and LHC energies ranging from $\sqrt{s} = 23.4$ GeV up to 13 TeV, with $\alpha = 0.9$ fixed. Solid black lines indicate the fitted region, in each case the CL is in the acceptable $99.9\% > \text{CL} > 0.1\%$ range. Dashed line indicates an extrapolation outside the fitted region. These results are detailed in Appendix C and further explained in terms of a proton substructure in Subsection 3.4. The dashed lines continue the fitted, solid curves outside the fitted region, to improve the clarity of the presentation.

2.3 Shadow profile functions

Turning to the impact parameter space, we get

$$t_{el}(b) = \int \frac{d^2\vec{\Delta}}{(2\pi)^2}\, e^{-i\vec{\Delta}\vec{b}}\, T_{el}(\Delta) = \frac{1}{2\pi}\int J_0(\Delta\, b)\, T_{el}(\Delta)\, \Delta\, d\Delta\,, \quad \Delta \equiv |\vec{\Delta}|\,, \quad b \equiv |\vec{b}|\,, \tag{2.25}$$

This Fourier-transformed elastic amplitude $t_{el}(b)$ can be represented in the eikonal form

$$t_{el}(b) = i\left[1 - e^{-\Omega(b)}\right]\,, \tag{2.26}$$

where $\Omega(b)$ is the so-called opacity function, which is in general complex. Thus, a statistically acceptable description of the elastic scattering data provides us with a direct access to the

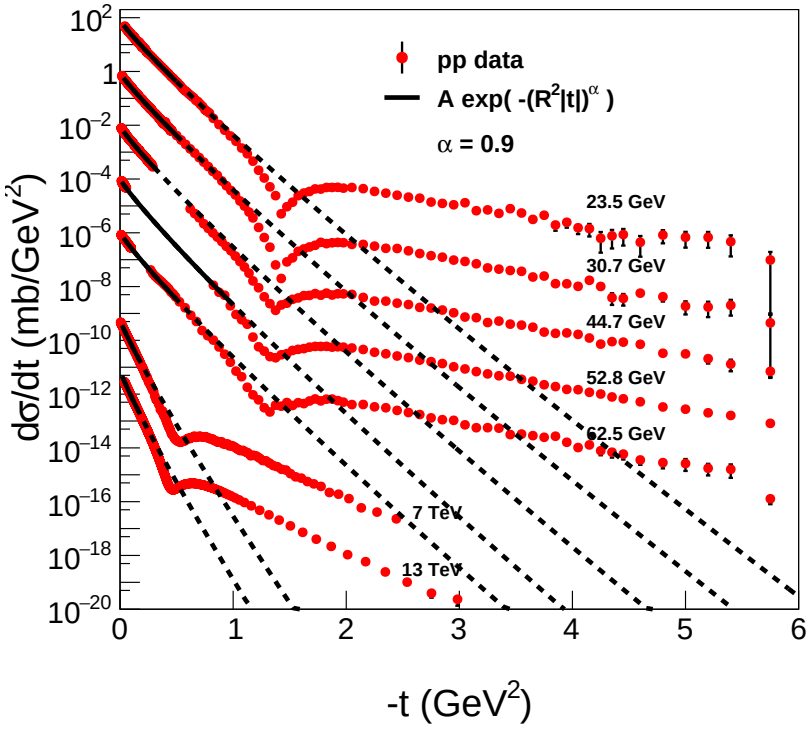


Figure 7. Summary plot of the Lévy fits, $d\sigma/dt = A\exp(-(R^2|t|)^\alpha)$ to the cone (or low-$|t|$) region of the elastic pp scattering data at ISR and LHC energies ranging from $\sqrt{s} = 23.4$ GeV to 13 TeV, with $\alpha = 0.9$ fixed. The dashed lines continue the fitted, solid curves outside the fitted region, to improve the clarity of the presentation.

opacity $\Omega(b)$ (known also as the eikonal function) and, in particular, to the shadow profile function defined as

$$P(b) = 1 - \left|e^{-\Omega(b)}\right|^2 . \tag{2.27}$$

In this paper, we find the best fits to elastic pp and $p\bar{p}$ differential cross-sections and evaluate the slope parameters and the shadow profiles to find their excitation functions, as described in the next section.

3 Data analysis

Let us test the power of our Lévy expansion method first on the already published differential cross-section data of elastic pp collisions at $\sqrt{s} = 7$ TeV, utilizing the published TOTEM data set of Ref. [32]. Fig. 2 indicates that the 7 TeV TOTEM data set can be represented by a fourth-order Lévy expansion with a reasonable $\chi^2/\text{NDF} = 234/157$, that corresponds to a

marginal confidence level of CL $\simeq 2 \times 10^{-5}$. Inspecting Fig. 2 by eye suggests also that the parameters of the Lévy expansion in Eq. (2.1) can be interpreted as they closely represent the data. These parameters are printed on the right-hand side of the top panel of Figs. 2–3. The first parameter is the Lévy scale parameter $R \simeq 0.63$ fm, which is a characteristic Lévy scale of the proton.

To gain intuition about the meaning of R, before we go deeper to the data analysis, let us consider first the usual $\alpha = 1$ case, neglecting all but the leading order (unity) term in the series that defines the Lévy expansion of the differential cross-section in Eq. (2.1).

In this Gaussian case, the differential cross section is apparently a structureless exponential in t,

$$\frac{d\sigma}{dt} = A \exp(-R^2|t|) \,, \tag{3.1}$$

that corresponds to a Gaussian parametrization of the forward scattering amplitude, based on Eq. (2.17):

$$t_{el}(b) \propto \exp\left(-\frac{b^2}{2R^2}\right) . \tag{3.2}$$

The Gaussian distributions correspond to central limit theorems, when several random elementary processes are convoluted to yield the final distribution. The Gaussian appears as a limiting distribution, if the elementary processes have finite means and variances, regardless of further details of the elementary probability distributions. Generalized central limit theorems describe limiting distributions for a large number of elementary processes, when the resulting elementary distributions have infinite means or variances. In these cases a limiting distribution exists, that remains stable for adding one more random elementary process. Due to this reason, such distributions are called stable, or, Lévy-stable distributions. They are denoted by $S_n(x|\alpha_L, \beta, \gamma, \delta)$ where x is the variable of the distribution, α_L stands for the Lévy index of stability, β is the asymmetry parameter, γ is the so called scale parameter, and δ is the location parameter of this distribution, while n determines the convention [20, 28]. In this paper, we follow the conventions defined in Ref. [20], that correspond to $n = 2$. In this case, for $\alpha \neq 1$, the Fourier-transformed Lévy stable source distribution reads as

$$\tilde{S}_2(q|\alpha_L, \beta, \gamma, \delta) = \exp\left(iq\delta - \gamma^{\alpha_L} q^{\alpha_L} \left[1 - i\beta \,\mathrm{sgn}(u) \tan(\frac{1}{2}\pi\alpha_L)\right]\right) . \tag{3.3}$$

By now, the Lévy stable distributions are implemented into commercially available software packages, for example, Mathematica. In practice, we utilize the parameterization that is continuous in the Lévy index of stability α_L [27]. Given that the Gaussians correspond to Lévy-stable source distributions with $\alpha_L = 2$ (the value of the exponent in the Fourier-transformed Gaussians) and taking into account, that in our analysis the Gaussian elastic amplitude $t_{el}(b)$ has the exponent $\alpha = 1$, we conclude that the Lévy index of stability α_L is simply twice the exponent of our Lévy series, i.e.

$$\alpha_L = 2\alpha \,. \tag{3.4}$$

Recently, the TOTEM Collaboration published a high precision measurement of the low-$|t|$ region of the differential cross-section of elastic pp scattering at $\sqrt{s} = 8$ TeV [25]. This demonstrated a significant, more than 7 σ deviation from a simple exponential cone behaviour, corresponding to a Gaussian representation of the forward scattering amplitude. In our language, this means that $\alpha < 1$, or, using the standard form of the Lévy index of stability, $\alpha_L = 2\alpha < 2$.

Let us also investigate in detail the recently released, new 13 TeV TOTEM preliminary data set [19], to look for charge (C) odd effects in the comparison of elastic pp and $p\bar{p}$ collisions. In what follows, we consider four different aspects of the TOTEM data in comparison with elastic scattering data at lower energies, both for pp and $p\bar{p}$ collisions. Namely, we compare the shadow profile functions, the t-dependence of the elastic slope parameter B, the same for the ρ-parameter and the so-called nuclear phase $\phi(t)$, that measures the argument of the nuclear forward scattering amplitude. Finally, we show in a simple and straightforward analysis of a large-$|t|$ region beyond the diffractive minimum and maximum, that the differential cross-section of elastic pp scattering evidences a proton substructure of two distinct sizes for GeV and TeV energy ranges, respectively.

3.1 Looking for Odderon effects

As noted in Refs. [4, 33], the only direct way to see the Odderon is by comparing the particle and antiparticle scattering at sufficiently high energies provided that the high-energy pp and $p\bar{p}$ elastic scattering amplitude is a difference or a sum of even and odd C-parity contributions. The even-under-crossing part consists of the Pomeron and the f Reggeon trajectory, while the odd-under-crossing part contains the Odderon and a contribution from the ω Reggeon, i.e.

$$T_{el}^{pp}(s,t) = T_{el}^{+}(s,t) + T_{el}^{-}(s,t), \tag{3.5}$$

$$T_{el}^{p\bar{p}}(s,t) = T_{el}^{+}(s,t) - T_{el}^{-}(s,t), \tag{3.6}$$

$$T_{el}^{+}(s,t) = T_{el}^{P}(s,t) + T_{el}^{f}(s,t), \tag{3.7}$$

$$T_{el}^{-}(s,t) = T_{el}^{O}(s,t) + T_{el}^{\omega}(s,t)\,. \tag{3.8}$$

It is clear from the above formulae that the odd component of the amplitude can be extracted from the difference of the antipp and the pp scattering amplitudes. At sufficiently high energies, the relative contributions from secondary Regge trajectories is suppressed, as they decay as negative powers of the colliding energy $\sqrt{s}$. The vanishing nature of these Reggeon contributions offers a direct way of extracting the Odderon as well as the Pomeron contributions, $T_{el}^{O}(s,t)$ and $T_{el}^{P}(s,t)$, respectively, from the elastic scattering data at sufficiently high colliding energies.

In Refs. [4], the authors argued that the LHC energy scale is already sufficiently large to suppress the Reggeon contributions, and they presented the (s,t)-dependent contributions of an Odderon exchange to the differential and total cross-sections at LHC energies. That

analysis, however, relied on a model-dependent, phenomenological extension of the Phillips-Barger model [34] and focussed on fitting the dip region of elastic pp scattering, but it did not analyse in detail the tail and cone regions. In fact, that analysis relied heavily on the extrapolation of fitted model parameters of pp and $p\bar{p}$ reactions to exactly the same energies. Similarly, Ref. [13] also argued that the currently highest LHC energy of $\sqrt{s} = 13$ TeV is sufficiently high to see the Odderon contribution, given that the Pomeron and the Odderon contributions can be extracted from the forward scattering amplitudes at sufficiently high energies as

$$T_{el}^{P}(s,t) \simeq \frac{1}{2}\left(T_{el}^{pp}(s,t) + T_{el}^{p\bar{p}}(s,t)\right), \tag{3.9}$$

$$T_{el}^{O}(s,t) \simeq \frac{1}{2}\left(T_{el}^{pp}(s,t) - T_{el}^{p\bar{p}}(s,t)\right). \tag{3.10}$$

One of the problems is that the elastic pp and $p\bar{p}$ scattering data have not been measured at the same energies in the TeV region so far. So, we strongly emphasize the need to run the LHC accelerator at the highest Tevatron energies of 1.96 TeV, in order to make such direct comparisons possible. Another problem is a lack of precision data at the low- and high-$|t|$, primarily, in $p\bar{p}$ collisions. Nevertheless, we show that robust features of the already performed measurements provide not only an Odderon signal, but they also indicate the existence of a proton substructure.

In this paper, we take the data as given and do not attempt to extrapolate the model parameters for their unmeasured values. Instead, we look for even-under-crossing and odd-under-crossing contributions by comparing pp and $p\bar{p}$ collisions at different energies, looking for robust features that can be extracted in a model-independent manner. In addition, we build upon Ref. [4] by assuming, as justified by that analysis, that the Reggeon contributions to the forward scattering amplitudes are negligible if $\sqrt{s} \geq 1.96$ TeV.

Let us first of all compare the behaviour of the shadow profile functions $P(b)$ before investigating the four-momentum transfer dependent $B(t)$ functions for both pp and $p\bar{p}$ reactions.

3.2 Excitation function of the shadow profiles

The excitation of the shadow profiles is obtained from the forward scattering amplitude obtained by fits to pp elastic scattering cross-section data from $\sqrt{s} = 23.4$ GeV till 13 TeV, as illustrated in Fig. 8. The excitation function of the shadow profile functions for $p\bar{p}$ reactions is indicated in Fig. 9.

In pp collisions at the lower ISR energies, the shadow profile functions look nearly Gaussian, and their values at zero impact parameter are below unity, $P(b = 0) < 1$. The picture changes at the LHC energies of 7 and 13 TeV, where the shadow profile functions seem to saturate, with $P(b = 0) > 99.9\%$ in an extended range, for $b < 0.4$ fm at 7 TeV and $b < 0.5$ fm at 13 TeV. This indicates that the black disc limit is reached in the center of these collisions, corresponding to $P(b) \approx 1$. However, outside the 0.4 or 0.5 fm saturated regions, the $P(b)$ decreases nearly in the same manner, as at lower energies. One may conclude that a

new, black region opens up in the TeV energy region, which increases with growing colliding energies, and it is surrounded by a gray hair or skin region, that has a "skin-width" that is approximately independent of the energy of the colliding protons. Thus, with an increase of colliding energies, the protons become blacker, they do not become edgier but become larger. This is the so called BnEL effect [35], which can be contrasted to the earlier expectations, the so-called BEL effect suggesting that with increasing energy of the collisions, the protons might become blacker, edgier and larger.

A new trend opens up with the 7 TeV TOTEM data, that indicates a black region, $P(b) \simeq 1$ up to a radius of about 0.4 fm and the size of this black region is increasing with an increase of colliding energies. Note also that at the ISR energy range, $\sqrt{s} \leq 62$ GeV, the shadow profiles are very similar, however, at the TeV energy range, pp and $p\bar{p}$ collisions evolve somewhat differently. For example, in the shadow-profile of the elastic $p\bar{p}$ collisions at $\sqrt{s} = 1.96$ TeV, the nearly flat region with $P(b) \approx 1$ is not yet present, while this region is present and it is rather extended in the shadow profiles of elastic pp collisions at $\sqrt{s} = 7$ and 13 TeV.

In both Figs. 8 and 9, one can observe that the proton becomes blacker and larger with increasing energies, however, its edge is apparently nearly constant, looks like a nuclear skin that has the same skin-width regardless of the energy of the collision. These results are similar to earlier observations, published in Refs. [35–38].

To highlight this point, we have evaluated the difference between the shadow profile functions $P(b|pp, 13\,\text{TeV}) - P(b|pp, 7\,\text{TeV})$, shown in Fig. 10, that contains only effects that come from evolution of the structure of the proton with increasing $\sqrt{s}$. This energy-dependent evolution of the shadow profile can be compared to the difference of the shadow profile of pp collisions at 7 TeV and that of $p\bar{p}$ collisions at the lower $\sqrt{s} = 1.96$ TeV, $P(b|pp, 7\,\text{TeV}) - P(b|p\bar{p}, 1.96\,\text{TeV})$, also shown in Fig. 10. We find that the energy evolution of the shadow profiles is similar for the C-even pp collisions and for the C-odd $p\bar{p}$ collisions.

We summarize that from the shadow profile functions it is very difficult to draw strong conclusions given that the model-independent method does not allow estimation of the collision energy dependence of the model parameters yet, so it is very hard to tell if the obvious difference between the pp and the $p\bar{p}$ collisions is due to the difference in the energy of the collisions or not.

This observation underlines the importance of data-taking at the LHC, a pp collider, with $\sqrt{s}$ decreased to as close as reasonably possible to 1.96 TeV or 1.8 TeV, the energy range of the $p\bar{p}$ collisions measured at Tevatron.

3.3 Results for the nuclear slope parameter

Let us move on to the analysis of another important characteristics, namely, the t-dependent nuclear slope $B(t)$.

In pp collisions, the analysis of the four-momentum transfer and center-of-mass energy dependent nuclear slope, $B(t, s)$ is summarized in Fig. 11. Surprisingly, in the low-$|t|$ region,

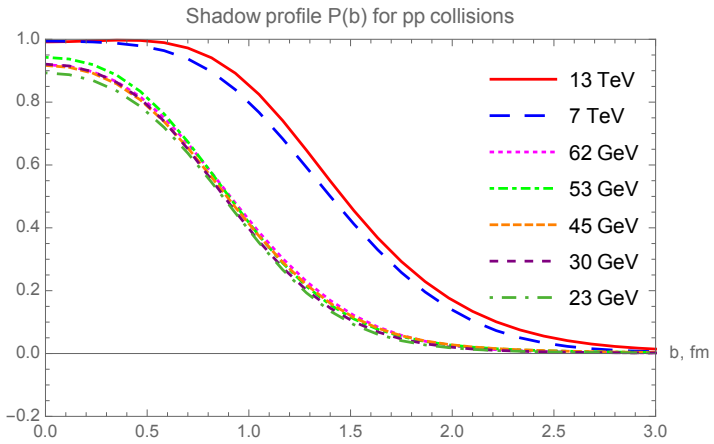


Figure 8. Shadow profile functions for pp collisions from $\sqrt{s} = 23.4$ GeV to 13 TeV.

where a diffraction cone is expected, we find that $B(t)$ is actually not exactly constant, but a t-dependent function, so the exponential behaviour can only be considered as an approximation, as clearly shown in Fig. 11. In the ISR energy range 23.5 GeV $\leq \sqrt{s} \leq$ 62.5 GeV, the nuclear slope can be considered as roughly constant both in the $|t| \leq 1.0$ GeV^2 (diffractive cone) and in the $2.0 \leq |t| \leq 3.0$ GeV^2 (tail) region, with nearly ISR energy independent $B_{\rm cone}(pp|{\rm ISR}) \approx 10$ GeV^{-2} and $B_{\rm tail}(pp|{\rm ISR}) \approx 2$ GeV^{-2}, rather surprisingly. At the LHC energy scales $\sqrt{s}$ =7 and 13 TeV, the cone region shrinks, as expected, down to $|t| \leq 0.3$ GeV^2, however, rather unexpectedly and surprisingly, the tail region opens up with a featureless, nearly flat $B(t)$ function that extends the tail region to $1.0 \leq |t| \leq 3.0$ GeV^2. An obvious and numerically very

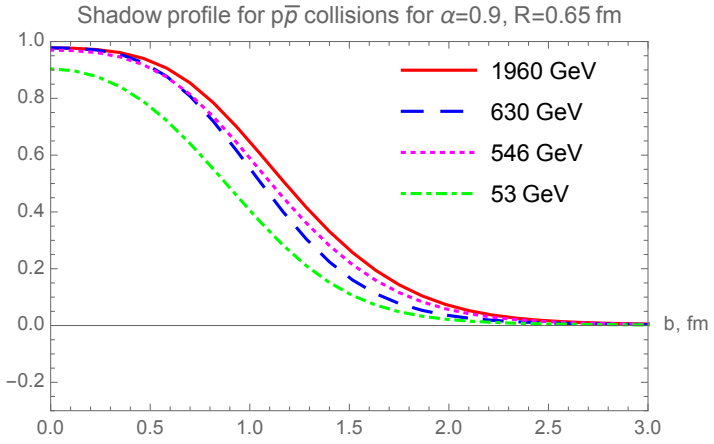


Figure 9. Shadow profiles for $p\bar{p}$ collisions, $\sqrt{s} = 53$ GeV to 1.96 TeV.

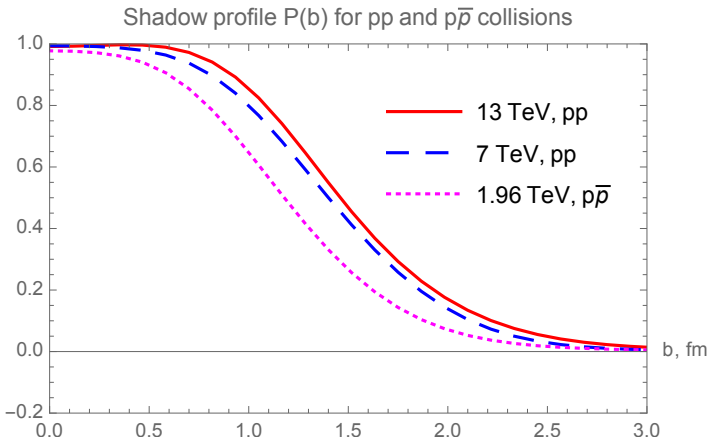


Figure 10. Shadow profile functions of pp collisions at $\sqrt{s} = 13$ and 7 TeV, as compared to the shadow profile function for $\sqrt{s} = 1.96$ TeV $p\bar{p}$ collisions.

stable observation is that the low-$|t|$ approximate value, $B_{\rm cone}(pp|{\rm LHC}) \approx 20$ GeV^2 is nearly a factor of two larger than the corresponding values at ISR, but also it is clear that these values are significantly t-dependent. On the other hand, in the large-$|t|$ region, $B_{\rm tail}(pp|{\rm LHC}) \approx 5$ GeV^{-2}, valid in a broad, 2 GeV^{-2} wide range of $|t|$, with not larger than 20 % level variations over this range.

It is important to realize, that the asymptotic value $B_{\rm tail}(pp|{\rm LHC}) \approx 5$ GeV^2 is nearly independent of the 7 or 13 TeV colliding energies and it is apparently significantly larger than the same asymptotic values at the ISR energies. It is rather clear that these values of $B(t)$, nearly constant over such rather extended 1 or 2 GeV^2 ranges (plateaux) of $|t|$, indicate two different and nearly Gaussian shaped structures, the proton "shell" and a newly found proton substructure already mentioned above.

In $p\bar{p}$ elastic collisions, a similar analysis of the four-momentum transfer squared and center-of-mass energy dependent nuclear slope, $B(t, s)$ is summarized in Fig. 12. In this analysis, the data are less detailed and only one data set is analyzed in the ISR energy range, corresponding to $\sqrt{s} = 53$ GeV. This data set has points both in the cone and in the tail regions, while the dataset at $\sqrt{s} = 546$ GeV is detailed in the low-$|t|$ region but lacks data in the tail. The data at $\sqrt{s} = 630$ GeV lacks data in the cone region, but extends more to the tail range, finally the data that we analyze at the Tevatron energy scale, at $\sqrt{s} = 1.96$ TeV, have limited $|t|$-range that only partially covers the cone and the tail regions.

For a kind of uniformity of the comparisons of $p\bar{p}$ elastic scattering data at various energies, we thus rely on fits and extrapolations with fixed $\alpha = 0.9$ and $R = 0.65$ fm, as detailed in Appendix B, and also summarized in Fig. 5. In the low-$|t|$ region, where a diffractive cone is expected, we find that $B(t)$ is actually not exactly constant, but a t-dependent function, so the exponential behaviour can only be considered as an approximation

at all the considered energies, as clearly seen in Fig. 12. In $p\bar{p}$ collisions, the nuclear slope is approximately a constant both in the $|t| \leq 0.5$ GeV^2 (cone), as well as in the $2.0 \leq |t| \leq 3.0$ GeV^2 (tail) region. These data sets cover a broad energy range, and Fig. 12 clearly indicates, that approximate average values of $B_{\rm cone}(p\bar{p})$ increase monotonically with an increase of $\sqrt{s}$. It is remarkable, that the slope parameter $B(t)$ is, rather surprisingly, tending to an energy-scale independent asymptotic value of $B_{\rm tail}(p\bar{p}) \approx 5$ GeV^{-2}, a value that is (within the errors) the same as the slope of the tail at the LHC energies. The range, over which the asymptotic exponential region prevails, is apparently extending at least up to 3 GeV^2 or more. The larger the colliding energy, the broader this region, which starts to open at $|t| \simeq 1.5$ GeV^2 at $\sqrt{s} = 1.96$ TeV. Thus, the asymptotic value $B_{\rm tail}(p\bar{p}) \approx 5$ GeV^2 is nearly independent of the 1.96, 7 or 13 TeV colliding energies and is almost independent of the type of the collisions as well.

It is clear that these two different, but nearly constant asymptotic values of $B(t)$, corresponding to $B_{\rm tail}(p\bar{p}) \approx B_{\rm tail}(pp|{\rm LHC}) \approx 5$ GeV^{-2} and $B_{\rm tail}(pp|{\rm ISR}) \approx 2$ GeV^{-2} over extended, 1 or 2 GeV^2 wide four-momentum transfer squared ranges exhibit a domain with a nearly $\exp(-B|t|)$ behaviour. Thus, this domain reveals the existence of a proton substructure with a nearly Gaussian elastic scattering amplitude distribution, $t_{el}(b) \propto \exp(-b^2/(2R^2))$. As is well known, an approximate value of the slope parameter $B_{\rm tail}$ is proportional to the squared Gaussian radius of such a substructure. The larger radius of this substructure is observed in the TeV energy range, both in pp and in $p\bar{p}$ collisions, while a smaller-size substructure is seen in pp collisions in the $\sqrt{s} = 23.6 - 62.5$ GeV ISR energy range. From the relation $R^2\pi = 4\pi B$ (in natural units) [24, 39], the Gaussian radius of the substructure is about $R_{\rm LHC} \approx 0.9$ fm (TeV energies) and $R_{\rm ISR} \approx 0.6$ fm (GeV energies). The analysis of the proton substructure and the determination of its contribution to the total cross-section is detailed in the next subsection, as well as in Appendix C.

The values $R_{\rm LHC}$ and $R_{\rm ISR}$ are strikingly similar to the radii of an effective diquark (R_d) and quark (R_q), respectively, that were independently obtained to characterize the substructures inside the protons in Ref. [35]. It turned out that the unitarized quark-diquark model of elastic pp scattering (called the Real Extended Bialas-Bzdak or ReBB model) predicted the $\sqrt{s}$ dependence of the total cross-section, the dip position and even certain scaling properties of the differential cross-section of elastic pp scattering at $\sqrt{s} = 13$ TeV with a reasonably good accuracy, based on its tuning at ISR energies and the TOTEM data set at $\sqrt{s} = 7$ TeV. So, the hypothesis about a proton substructure gains a larger weight and evidence in our analysis and, thus, definitely deserves more detailed investigations – that, however, go beyond the scope of the model-independent approach elaborated in this work. In particular, an important question is whether the observed two distinct scales $R_{\rm LHC}$ and $R_{\rm ISR}$ correspond to the dressed diquark and the dressed quark, respectively, or simply represent a single substructure whose size grows with energy, remains open.

A dynamical model for the elastic amplitude based upon a two-scale structure of the proton was previously proposed also in Refs. [40–42]. In this model, while the first scale was associated with the confinement radius $R_c \simeq 1$ fm and can be attributed to the proton

"shell", the second semi-hard scale $r_0 \approx 0.3$ fm originates due to non-perturbative interactions of gluons and characterizes an effective gluonic "spot", or a cloud, around each of the valence quarks. Despite somewhat different values of the physical scales adopted in this model, it has appeared to predict the energy dependence of the total and elastic cross sections quite accurately, at least, in a parameter-dependent way. In our current work, however, instead of reviewing various possible model interpretations, we study the model-independent properties of the elastic scattering data and search for C-odd (or Odderon) effects. We employ our model-independent imaging method to sharpen the picture of the proton as can be "seen" by elastic scattering measurements at different energies.

We can observe in Fig. 11, that in pp collisions $B(t)$ starts in the cone region with nearly constant values. However, after the cone region, $B(t)$ starts to fall sharply, to cut through the $B(t) = 0$ line and to reach a deep minimum with $B(t) \ll 0$ values. Then this function starts to increase, it cuts through the $B(t) = 0$ line second time, from below, approaching its asymptotic value, $B_{\rm tail}$.

Remarkably, for $p\bar{p}$ collisions, the $B(t)$ functions behave apparently in a qualitatively different way. In this case, after the cone region, $B(t)$ approaches zero and it may marginally cross zero, but not so deeply and sharply as in the case of pp collisions. Taking into account that the published error on B in $p\bar{p}$ collisions is about 0.5 GeV^{-2} [43], the error on the extrapolated $B(t)$ function can be estimated also. The latter appears to be similar or even larger as compared to the error of B at the optical point $t = 0$. So it seems to us, that the crossing of the $B(t)$ function below zero is within errors and thus it is likely not a significant effect in any of the $p\bar{p}$ collision data.

To clarify this point more, we compare the $B(t)$ functions for pp collisions at $\sqrt{s} = 7$ and 13 TeV with that of the $p\bar{p}$ collisions at $\sqrt{s} = 1.96$ TeV, see Fig. 13. The nuclear slope in pp collisions becomes clearly and significantly negative in an extended $|t|$ region, starting from the diffractive minimum (dip) and lasting to the subsequent diffractive maximum (bump). These dip and bump structures are clearly visible in the corresponding data sets, as visualized in Figs. 3 and 2 as well. In contrast, for $p\bar{p}$ collisions in the Tevatron energy range, we do not find any dip and bump structure, that would correspond to a $|t|$-region where $B(t)$ were negative.

We have performed further tests to cross-check if, within the errors of the analysis, the dip and bump structure is indeed absent in $p\bar{p}$ collisions at $\sqrt{s} = 1.96$ TeV, or not. First of all, one can directly inspect Fig. 19 (bottom right) to see that any reasonably smooth (e.g. spline) extrapolation of the data points would lack a diffractive minimum structure. One may argue that we do not see the minimum because the values of α and R were fixed. However, these numbers specify the approximate Lévy shape only, $d\sigma/dt \propto \exp\left(-(R^2|t|)^\alpha\right)$, that decreases monotonically, so their variation cannot cause diffractive minima or maxima, as also apparent on the dashed lines of partial fits described in Appendices C and D. In any case, we have also tested numerically that changing α in the region of fixed 0.8 – 1.0 does not qualitatively change the behaviour of $B(t)$. Within the allowed range of variation of the essential Levy expansion parameters c_i, we find that the diffractive minimum is lacking in

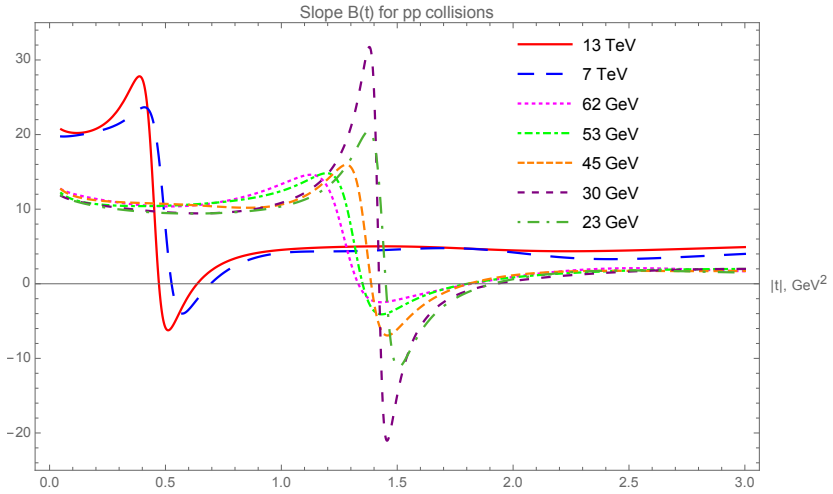


Figure 11. Slope parameter $B(t)$ for elastic pp collisions. The diffractive minimum followed by a diffractive maximum is present in each case, as evidenced by $B(t)$ crossing the $B(t) = 0$ line twice in each case.

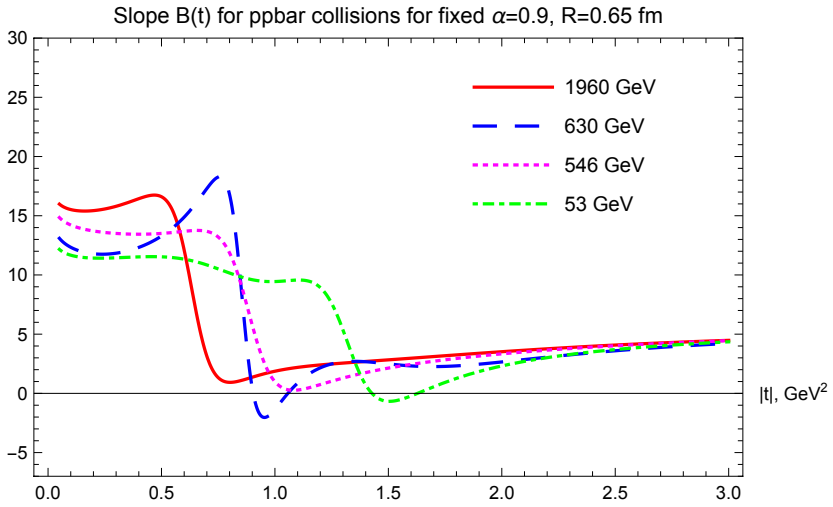


Figure 12. Slope parameter $B(t)$ for elastic $p\bar{p}$ collisions.

elastic $p\bar{p}$ collisions at 1.96 TeV.

This lack of diffractive minimum as well as the lack of the subsequent diffractive maximum in elastic $p\bar{p}$ collisions is contrasted to the strong diffractive minimum and maximum (the dip and bump structure) in elastic pp collisions at all investigated energies, hence it indicates a rather evident C-odd contribution to the forward scattering amplitude, the so called Odderon effect, shown also in Fig. 13.

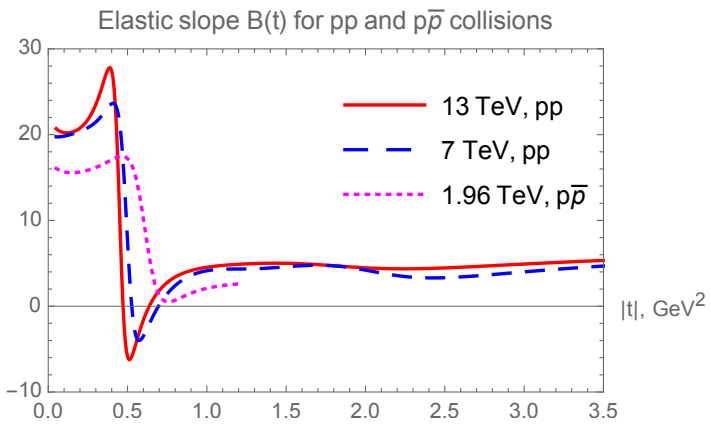


Figure 13. Slope parameter $B(t)$ for elastic pp collisions at $\sqrt{s} = 13$ and 7 TeV, compared to the slope parameter of $p\bar{p}$ collisions at $\sqrt{s} = 1.96$ TeV.

3.4 Evidence for proton substructure

Lévy fits to the tails of the differential cross-section of pp elastic scattering data from $\sqrt{s} =$ 23.5 GeV to 13 TeV are shown on a summary plot in Fig. 6. Note, that all the tails of the differential cross-sections are nearly linear on a log-linear plot, indicating a nearly Gaussian substructure of the proton. As was discussed earlier, two distinct sizes of such a substructure are seen, given the two different values of the slope in the ISR energy range of $\sqrt{s} = 23.5 - 62.5$ GeV, and in the LHC energy range of $\sqrt{s} = 7 - 13$ TeV. After the dip-bump structure, the differential cross-section of elastic pp collisions can be described by a simple $A \exp\left(-(|t|R^2)^\alpha\right)$ form, with $\alpha = 0.9 \pm 0.1$ value. Thus, for illustration this plot was done for fixed value of $\alpha = 0.9$.

We found that in the $23.5 \leq \sqrt{s} \leq 62.5$ GeV range, a proton substructure of nearly constant size (within errors) was present, with a characteristic Lévy length scale of $R_{\rm ISR} = 0.3 \pm 0.1$ fm, and with the corresponding contribution to the total cross-section $\sigma_{\rm ISR} = 0.3^{+0.3}_{-0.1}$ mb, where the quoted errors take into account also the errors coming from the variation of the value of α between 0.8 and 1.0 (see also the ISR plots in Fig. 20).

Fig. 14 indicates the TOTEM preliminary elastic scattering data at $\sqrt{s} = 13$ TeV with their fourth-order Lévy expansion fits. A power-law tail would show up as a straight line on this plot, but apparently it does not yet show up on the currently available $|t|$-range that extends up to about $t_{\rm max} = 4$ GeV^2. Although a straight line fit to the tail of this distribution is perhaps possible starting from $|t| \geq 2$ GeV^2, these points are getting close to the end of the TOTEM acceptance for this data set, and the error bars are getting large. To clarify the existence of such a possible power-law tail, more data at larger values of $|t|$ would be desirable. In contrast, the data in the well measurable $|t|$-range are sufficient to demonstrate the nearly exponential behaviour of the differential cross-section in the tail region that follows the dip and bump structure. The existence of the nearly Gaussian substructure is thus an

obvious and rather robust feature of the data (for more details, see Appendix C). This claim is also supported by the nearly energy- and t-independent values of the slope-parameter $B(t)$ in the tail regions, see Figs. 11 and 12.

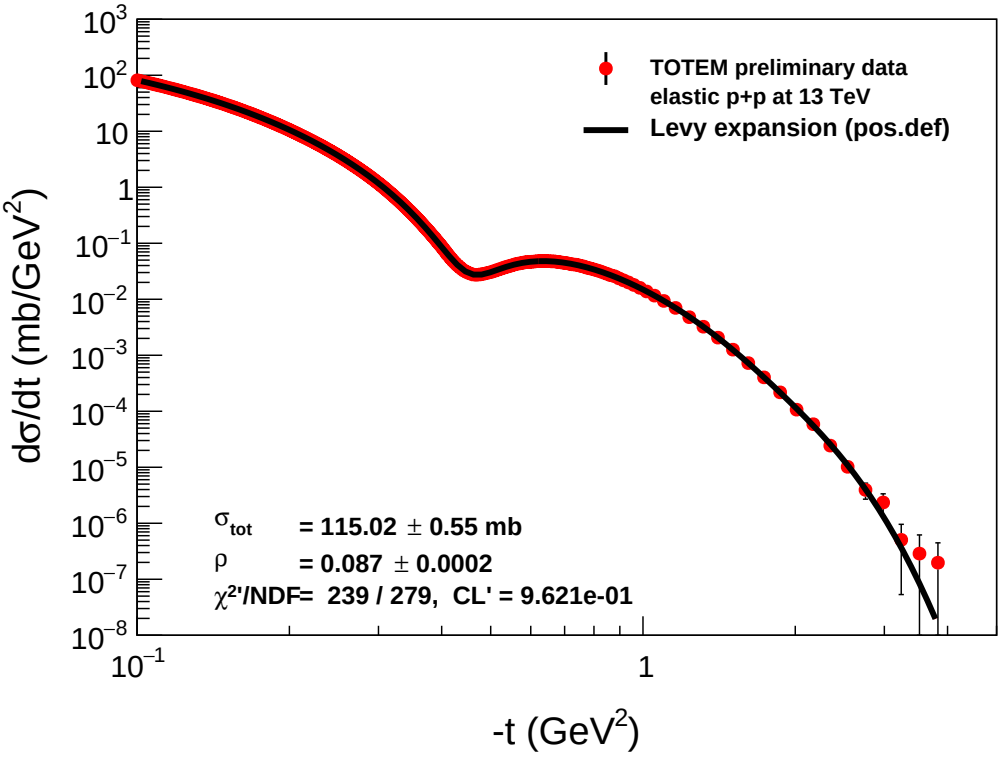


Figure 14. TOTEM preliminary data at $\sqrt{s} = 13$ TeV with their fourth-order Lévy expansion fits on a log-log plot. A power-law tail would show up as a straight line on this plot.

3.5 Results for $\rho(t)$

By reconstructing the forward scattering amplitude from the data, we have also found the t-dependent ratio of its real to the imaginary parts in pp collisions, the ρ-parameter Such a result is illustrated in Fig. 15 and indicates that the ρ-parameter is significantly t-dependent. This dependence is initially nearly linear in t. However, at the 7 and 13 TeV LHC energies, $\rho(t)$ starts to diverge to minus infinity which corresponds to a zero point or node of its imaginary part. Instead, we decided to analyze in greater detail the nuclear phase $\phi(t)$, the argument of the complex forward scattering amplitude T_{el}, that is traditionally measured in units of π, as described in the next subsection.

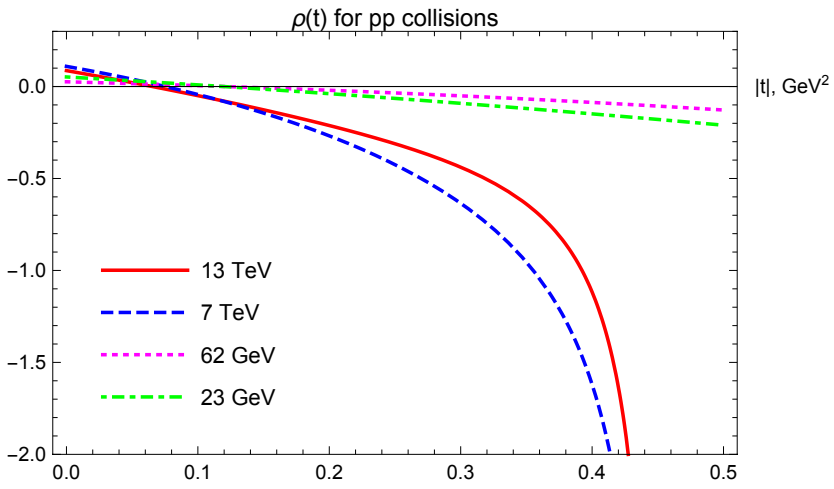


Figure 15. $\rho(t)$-parameter for pp elastic scattering collisions.

3.6 Results for the nuclear phase $\phi(t)$

In this subsection, let us investigate in detail if we can identify the Odderon effects in the t-dependence of the nuclear phase $\phi(t)$. As we clarify in Appendices A and B, such a phase can be reconstructed mostly from the differential cross-section at low-momentum transfers squared. In Appendix B we have demonstrated that $\rho(t = 0)$ cannot be reliably extracted from the studied elastic $p\bar{p}$ collision data, in particular, due to a significant lack of the low-$|t|$ data points. However, in Appendix A we demonstrated that $\rho(t)$ can be extracted from Lévy fits to elastic pp scattering, with the exception of $\sqrt{s} = 44.7$ GeV and 52.8 GeV data, where the confidence level of our fits is not in the statistically acceptable domain.

We have evaluated the t-dependent nuclear phase for pp collisions in the both ISR and LHC energy ranges. Unfortunately, the ISR range is a cumbersome one, where the Reggeon as well as the Pomeron and Odderon contributions mix with each other. In this energy range, for some of the pp collision data sets, we found a node at the same (or close) $|t|$ values above 1 GeV^2 while our sensitivity studies indicate that in this region our method to reconstruct the nuclear phase has increasing systematic difficulties. So, we cannot at present reliably test if the nodes of the nuclear phase coincide or not at low energies in pp and $p\bar{p}$ collisions. We can however make a statement that the pp collisions at the ISR energy range of $23.5 \leq \sqrt{s} \leq 62.5$ GeV, the nuclear phase does not reach zero for $|t| \leq 1$ GeV^2.

Fortunately, a similar analysis in the TeV energy range gave interesting results. Fig. 16 indicates that the phase $\phi(t)$ reaches the first zero at 7 and 13 TeV simultaneously at $|t_0|(pp) \approx 0.45 \pm 0.05$ GeV^2 in pp collisions, while the first zero of ϕ is reached at a rather different value of $|t_0|(p\bar{p}) \approx 0.70 \pm 0.05$ for 1.96 TeV $p\bar{p}$ collisions.

This is an important qualitative feature of $\phi(t)$, that indicates a significant Odderon contribution, that apparently cannot be attributed to an s-dependent effect, given that pp

collisions at $\sqrt{s} = 13$ and 7 TeV have the node where $\phi(t)$ jumps from π to zero practically at the same point. This subtle Odderon signature is clearly illustrated in Fig. 16 and cannot be directly seen in the differential cross sections. Thus, the $\sqrt{s}$ independence of the node (zero point) of the nuclear phase $\phi(t)$ in the TeV energy range for pp collisions and its strong shift in $p\bar{p}$ collisions in the TeV energy range, where the Reggeon contributions are apparently negligible, can be considered as a second reliable signature of the Odderon.

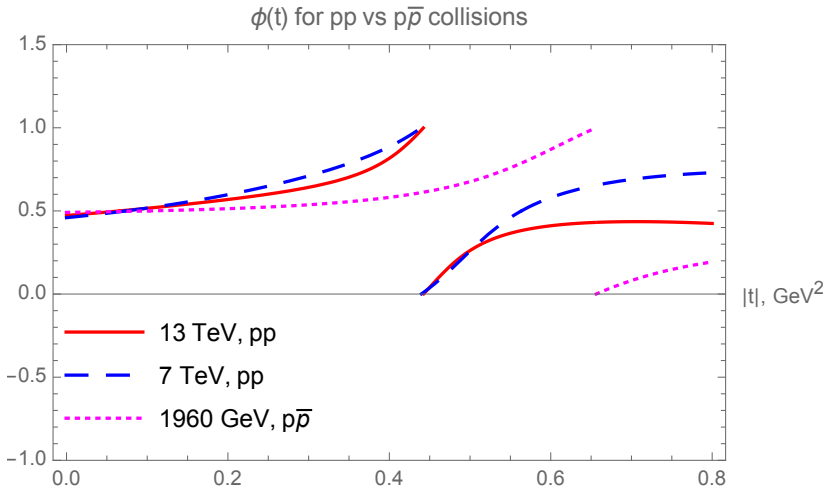


Figure 16. The nuclear phase $\phi(t)$, shown in units of π as a function of the four-momentum transfer squared $|t|$, for pp collisions at $\sqrt{s} = 13$ TeV and 7 TeV, as compared to the nuclear phase for $p\bar{p}$ collisions at $\sqrt{s} = 1.96$ TeV.

4 Discussion

Our experience is that many of our results, for example, for $\rho(t)$ and also for the nuclear phase $\phi(t)$ in the $|t| > 1$ GeV^2 region are very sensitive to the precise details of the fits, so interpretation of the TOTEM results at $\sqrt{s} = 13$ TeV depends critically and sensitively on the currently preliminary TOTEM data points and their error bars. Certain features of our analysis, for example, the behaviour of $B(t)$ in the range where the slopes could directly be evaluated from the data are more robust and stable.

Thus, we feel strongly motivated to warn the astute reader against the over-interpretation of model results that indicate certain features of the elastic scattering data correctly only on the qualitative level, but fail miserably on a confidence level test. Actually, the Odderon effects that we discuss in detail in this work are due to some robust and model independent features of the data, but we have investigated other more subtle effects too that we do not emphasize in this work.

Our key point is that the significance of the new Odderon effects can be revealed only if the data sets are final, with published statistical and systematic errors, and if they can be

correctly and faithfully represented by theoretical calculations. So we recommend to carefully evaluate the confidence levels of all subsequent theoretical analysis of final TOTEM data in future analyses and to determine the significance of the presence of novel effects like the Odderon contributions. Our method, presented in this work, allows for such sensitivity and significance analysis, however, given that the TOTEM data at $\sqrt{s} = 13$ TeV are preliminary, the evaluation of the systematic errors of the our fit results would most likely also be premature at present.

Nevertheless, we may warn the careful readers that descriptions of possible Odderon effects or the lack of them, based on data analysis with zero confidence levels might have apparently been over-interpreted recently: the significance of the interpretation of fits that do not describe the data in a statistically acceptable manner is not particularly well defined. Based on our experience, we recommend against the over-interpretation of the data in terms of models that do not have a confidence level of at least CL $\geq 10^{-5}$, but in a final analysis, we strongly recommend to rely on descriptions that have a confidence level of at least CL $> 0.1\%$ before the model results can be interpreted. The authors should also check if their optimization procedure has converged or not and test if the error matrix is accurate and the estimated distance to the real minimum is sufficiently small.

In our studies, we have found that small variations in the fit range or in the values of the fit parameters do not change the following robust features of the data, that we highlight below.

4.1 Qualitative features

While searching for the differences between the differential cross-sections of elastic pp and $p\bar{p}$ collisions, that could exhibit a C-odd contribution, or an Odderon effect in 13 TeV pp elastic scattering, we have evaluated the shadow profile functions at 7 and 13 TeV pp collisions using a novel imaging method, the model-independent Lévy expansion.

We have compared the shadow profile functions of pp and $p\bar{p}$ collisions at various energies. We have found that the shadow profiles saturate at the LHC energies of 7–13 TeV: for small values of the impact parameter, a $P(b) \simeq 1$ region opens up. With increasing the collision energies, the protons become blacker, but not edgier, and larger, confirming the BnEL effect, that was reported in Ref. [35].

We see a significant difference between the shadow profile functions $P(b)$ of protons and anti-protons in the TeV region, but from the current analysis we cannot determine uniquely, if this difference is an Odderon effect, or, an effect of saturation that is apparent also in pp collisions with an increase of collision energy. We would need pp and $p\bar{p}$ elastic scattering data at exactly the same collision energies, that can be realized these days only by running the LHC accelerator at energies close to the Tevatron energy scales of $\sqrt{s} = 1.8$ – 1.96 TeV.

In Subsection 2.2, we have analyzed the dependence of the B-slope parameter on the four-momentum transfer squared t in pp as well as in $p\bar{p}$ reactions. We have found, that the $B(t)$ functions indicate an Odderon effect very clearly.

Surprisingly, we have identified a $|t|$ region after the dip and the bump structure, where a clear-cut evidence is seen in our analysis for a proton substructure of two distinct sizes in two experimentally probed GeV and TeV energy ranges. In every case, such a substructure is characterized by a Lévy exponent of $\alpha = 0.9 \pm 0.1$. Possible evidence for a new substructure inside the proton at LHC energies was, as far as we know, first pointed out by Dremin in Ref. [16]. In this paper, we explored this possibility in detail and identified the characteristic Lévy exponent as $\alpha = 0.9 \pm 0.1$, characterized the substructure with an approximate Gaussian and Lévy scales at the ISR and LHC energies, respectively, and determined the corresponding contribution to the total pp cross-section as well, as described in Subsection 2.2 and in Appendix C. Based on the Gaussian sizes found in Subsection 2.2, it is tempting to note that they are strikingly similar to a dressed quark and a dressed diquark, found to describe elastic pp scattering in an earlier, model dependent analysis [35]. Their presence seems to provide a phenomenological support for the quark-diquark picture of the proton, which is deeply related to the solution of the confinement problem in QCD proposed recently by Brodsky and collaborators in Ref. [44]. This, however, does not exclude the possibility for a single substructure growing with energy. More measurements at intermediate energies (between ISR and LHC) would be strongly desirable to justify the quark-diquark picture or to prove a continuous growth of a single substructure (a dressed quark) with energy.

4.2 Highlighted results

Let us highlight some of the important points of our study:

1. We have found a solid, stable and clear-cut evidence for a proton substructure, with two different sizes extracted for two distinct (GeV and TeV) energy ranges that are similar to the sizes of a dressed quark and a dressed diquark, respectively, as discussed in Ref. [35], and as also derived from QCD in Ref. [44]. Fig. 13, even without the quantitative results, demonstrates the existence of such a proton substructure, corresponding to the second extended plateau in the large-$|t|$ region (besides the usual elastic cone region at low $|t|$) with a nearly exponential contribution to the differential cross-section of elastic pp scattering. We noticed that such a plateau corresponds to a dressed quark-scale substructure in the lower $\sqrt{s} = 23.5$ – 62.5 GeV energy range, while it resembles a larger, dressed diquark-scale substructure in the 7 – 13 TeV energy range, see Fig. 6. Whether this finding indeed corresponds to the existence of two different quark and diquark substructures, or a single (dressed-quark-like) substructure with an energy-dependent radius, is an open question.

2. At each energy and for each investigated data set, the forward scattering amplitude of elastic pp and $p\bar{p}$ collisions was described by our new Lévy series expansion method. With the help of the forward scattering amplitude, we have reconstructed values for the total cross-section and for the differential cross-section of elastic scattering. The published values of the total cross-sections were reproduced within errors and the fits to the differential cross-section looked fine. In case of several data sets they have also

passed the more stringent tests of mathematical statistics, namely the confidence level of most of our fits was not unacceptable from the point of view of mathematical statistics, either, with confidence levels CL > 0.1 %.

3. For all those data-sets, where the confidence level of the fit was not unacceptable from the point of view of mathematical statistics, we found that the exponent α was significantly less than unity in pp collisions, the deviation being a more than 5σ effect. Given that exponential behaviour corresponds to the case of $\alpha = 1$, and fits with CL > 0.1 % represent the data undoubtedly, we find that the differential cross-section at low $|t|$ is apparently non-exponential in 23.5, 30.7, 62.5 GeV and in 13 TeV pp elastic scattering data. It is quite remarkable, that the corresponding values of the non-exponentiality are $\alpha = 0.88 \pm 0.01$, 0.89 ± 0.02, 0.90 ± 0.01, 0.90 ± 0.01, when rounded up to two decimal digits. This implies that an average value of $\alpha = 0.89 \pm 0.02$ is consistent with all the measurements in a very broad energy range from 23.5 GeV to 13 TeV. The energy independence of this $\alpha = 0.89 \pm 0.02$ value calls for a physics interpretation, and for further studies.

4. Signals of non-exponentiality in the cone region are also indicated in $p\bar{p}$ elastic scattering data at all energies, where we have been able to describe all the analyzed datasets with an $\alpha = 0.9$ fixed value, from $\sqrt{s} = 53$ GeV to 1.96 TeV.

5. This non-exponential nature of the differential cross-section in the low-$|t|$ region implied that the slope parameter $B = B(t)$ is a function that is strongly dependent on the $|t|$ range, where it is determined. We have evaluated $B(t)$ both numerically and analytically in the whole $|t|$ region, where it is defined. The extrapolation of $B(t)$ to the optical point of $t = 0$ turned out to be model-dependent, not only due to the fact that there is a Coulomb effect that induces Coulomb-nuclear interference terms and modifies the slope at very small $|t|$, but also due to the analytic result that $\lim_{t\to 0} B(t) = \infty$, i.e. our Lévy expansion method is non-analytic at the optical point. This closely corresponds to the physical picture that we allow for the underlying source contributions that may have infinite root mean square, which is typical for a Lévy stable source distribution. (For a typical example, one may consider a Lorentzian distribution, that is a symmetric, Lévy stable distribution with Lévy index of stability $\alpha_L = 1$, corresponding to our non-exponential parameter $\alpha = 0.5$.

6. The lack of detailed data in the very low- or very large-$|t|$ regions in $p\bar{p}$ collisions prevented us to determine precisely the ρ and the B parameters of this case.

7. The analysis of the four-momentum transfer squared and the center of mass energy dependent nuclear slope, $B(t, s)$ in Fig. 11 not only confirms the existence of a proton substructure (corresponding to the existence of large regions in t where $B(t)$ is approximately but not exactly constant), but also indicates a sharp difference between the $B(t)$ functions of pp and $p\bar{p}$ collisions, when comparing Figs. 11 and 12. This is a clear-cut

and significant Odderon effect. For pp collisions, $B(t)$ starts with positive values, then it cuts sharply through the $B(t) = 0$ line and returns above it shortly but very significantly, corresponding to the dip and bump structure in the differential cross-section for elastic scattering in each of the investigated data sets. In contrast, in $p\bar{p}$ collisions, $B(t)$ approaches zero but within the errors of the analysis it does not cross it at $\sqrt{s} = 1.96$ TeV. At two of the lower energy scales of $\sqrt{s} = 630$ and 53 GeV, $B(t)$ apparently crosses zero and develops a minimum at $|t| = 2$ and 1 GeV^{-2}, respectively. However, taking into account that the published error on B in $p\bar{p}$ collisions is about 0.5 GeV^{-2} [43], the error on the extrapolated $B(t)$ function can be estimated to be similar or larger as compared to the error of B at the optical point of $t = 0$. So it seems to us, that the crossing of the $B(t)$ function below zero is within errors likely not a significant effect in any of the $p\bar{p}$ collision data. In the only data set that we could access in the TeV energy range, where the complicated Reggeon contributions are already negligible, $B(t)$ does not cross zero, so the diffractive minimum and maximum, the dip-bump structure is lacking in these$\sqrt{s} = 1.96$ TeV $p\bar{p}$ elastic collisions. Such a behaviour is in sharp contrast to the pp differential cross-sections at all energies. Apparently this is a clear-cut Odderon effect, as illustrated in Fig. 16.

8. In addition, we have also found a surprisingly clear Odderon effects in the t-dependent nuclear phase $\phi(t)$. Our analysis indicates that this phase becomes zero at the very different, high LHC energies of 7 and 13 TeV in elastic pp collisions at the same value of $|t_0| \approx 0.45$ GeV^2, that suggests that this $|t_0|$ value has a negligibly small dependence on the collision energy, $\sqrt{s}$. However, in elastic pp collisions at $\sqrt{s} = 1.96$ TeV, such a point of zero and subsequent discontinuity of the nuclear phase $\phi(t)$ is at a very different location from pp collisions.

9. We have also found a weak difference between the shadow profile functions $P(b)$ belonging to $p\bar{p}$ collisions at $\sqrt{s} = 1.96$ TeV as compared to that of pp collisions at 7 and 13 TeV. However, we also found a significant evolution of the shadow profile functions from 23.5 to 62.3 GeV and from 7 TeV to 13 TeV in elastic pp collisions.

10. In order to clarify if the difference between the shadow profiles of pp and $p\bar{p}$ collisions occurs due to the change of the colliding system type or due to the change of t he center of mass energy of the collisions, as well as to clarify differences of the other observables like $B(t)$ and $\phi(t)$, we strongly recommend to run the LHC measurements at lower energies, preferably in the vicinity of $\sqrt{s} = 1.96$ TeV, to measure the difference between pp and $p\bar{p}$ collisions exactly and to clarify the Odderon contribution without any possible energy evolution and extrapolation effects.

11. We recommend extreme care before drawing big conclusions, given that we see the sensitivity of some of the details like $\phi(t)$ at large $|t|$ for tiny details in the data and in changing some of the higher order coefficients of the fits. Possibly these tiny details differ

in some papers that may apparently draw big, but contradicting, and not particularly well founded conclusions about the existence or non-existence of the Odderon effects. When looking for a robust conclusion about the Odderon contribution, we recommend to look at the summary plot of the Lévy fits to the tails of the differential cross-sections of elastic scattering on a log-linear plot, as indicated in Fig. 13.

5 Summary and conclusions

In summary, we conclude that we have found clear-cut and post-factum rather obvious differences between the differential cross-sections of elastic pp and $p\bar{p}$ collisions, indicating a C-odd contribution: the Odderon effect. This corresponds to a small difference of the t-dependent slope parameters between pp collisions at 13 TeV and 7 TeV collision energies at the LHC as compared to a large change of the t-dependence of the slope parameter $B(t)$ in 1.96 TeV $p\bar{p}$ collisions. Another characteristic Odderon signal is the difference is between the existence of a diffractive minimum and maximum in both 13 and 7 TeV elastic pp scattering, corresponding to two distinct crossing-points of the $B(t)$ functions with the $B(t) = 0$ line, as contrasted to the monotonically decreasing differential cross-section of elastic $p\bar{p}$ collisions, with a t-dependent elastic slope that is $B(t) > 0$ significantly, a function that never crosses the $B(t) = 0$ line.

These Odderon signals, the change in $B(t)$ and the disappearance of the diffractive minimum as well as the diffractive maximum, when changing from pp reactions to $p\bar{p}$ reactions, are rather obvious, stable and clear-cut effects. Once they are identified, they can be directly seen on the data sets, when one plots the 13 TeV and 7 TeV differential cross-section of elastic pp scattering on the same plot with the differential cross-section of elastic $p\bar{p}$ scattering, as illustrated in Fig. 17.

We have confirmed such Odderon effects with a more refined and subtle analysis, that indicated the lack of energy dependence of the node $|t_0|$ of the nuclear phase $\phi(t)$ both in the TeV region $\phi(t) = 0$ at the same value of $|t_0|(pp) \approx 0.45 \pm 0.05$ GeV^2 both at 7 and 13 TeV. When evaluating the node of the nuclear phase for $p\bar{p}$ collisions at $\sqrt{s} = 1.96$ TeV, a significantly different value of $|t_0|(p\bar{p}) = 0.70 \pm 0.05$ GeV^2 was obtained for the position of this node. The difference between $|t_0|(pp)$ and $|t_0|(p\bar{p})$ is apparently a clear but subtle Odderon effect, that cannot be not obviously obtained by directly inspecting Fig. 17, but it supports the same conclusion about the presence of Odderon effects in the few TeV elastic scattering data.

As a by-product, but perhaps even more importantly, we have also found a clear-cut evidence for a proton substructure, as shown by the presence of the second, nearly exponential region in the differential cross-sections of elastic pp collisions at large $|t|$. At the ISR region, $23.4 \leq \sqrt{s} \leq 62$ GeV, from the asymptotic value of the t-dependent slope parameter of $B_{\rm ISR} \approx 2$ GeV^{-2} a substructure with a Gaussian radius of $R_{{\rm ISR},G} \approx 0.6$ fm, while at the LHC energies of $7 \leq \sqrt{s} \leq 13$ TeV, a substructure with a different Gaussian radius of $R_{{\rm LHC},G} \approx 0.9$ fm is identified. Apparently, the size of this structure found at the ISR and LHC matches

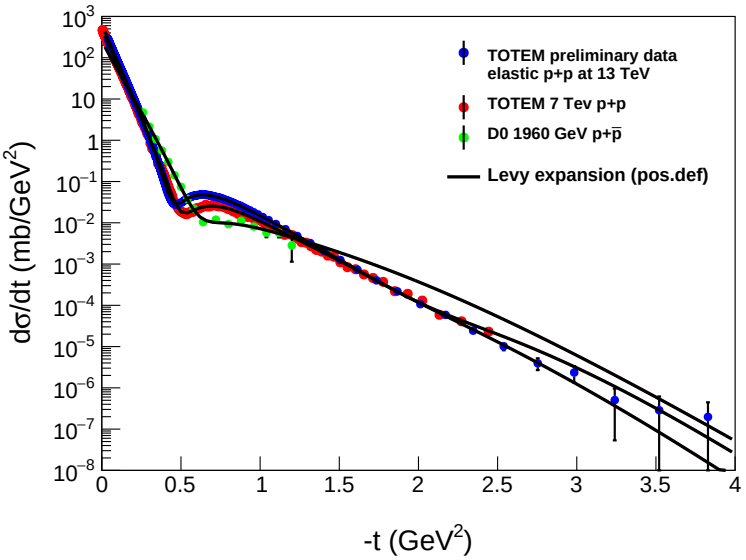


Figure 17. A direct comparison of the differential cross-sections of elastic pp scattering at the LHC energies of 7 and 13 TeV, with $p\bar{p}$ elastic scattering at the Tevatron energy of 1.96 TeV.

reasonably well the size of the dressed quarks and diquarks, respectively, as found recently in a unitarized Bialas-Bzak model analysis of 7 TeV elastic pp scattering [35]. These results may provide a phenomenological support for the quark-diquark picture of hadron confinement as obtained recently by Brodsky using AdS/QCD techniques [44], although they may not exclude the presence of a single dressed quark-like substructure with a continuously evolving (with energy) radius.

Our analysis indicates that the proton substructure contributes to the total pp cross-sections with $\sigma_{\rm ISR} = 0.3^{+0.3}_{-0.1}$ mb at ISR, and $\sigma_{\rm LHC} \approx 8.2^{+7.9}_{-4.7}$ mb at the LHC energies.

We have also found that this substructure can be better characterized by a Lévy source with $\alpha = 0.9$ as compared to a Gaussian source (corresponding to $\alpha = 1$). Using the characteristic Lévy length scale of $R_{{\rm ISR},L} = 0.3 \pm 0.1$ fm at ISR, and $R_{{\rm LHC},L} = 0.5 \pm 0.1$ fm at the LHC energies.

From the analysis of the cone region, we clearly demonstrated that the shape of the protons actually changes in the 7 – 13 TeV energy range, corresponding to an opening of a new channel, as clearly demonstrated by the appearance of a saturated $P(b) \approx 1$ region in the shadow profile functions in the TeV energy range.

Finally, based on our experience with precision description of the differential cross-sections of elastic pp and $p\bar{p}$ collisions let us warn the careful readers against over-interpreting fit results when the fitted function does not represent the data with a statistically not unacceptable confidence level.

We hope that this data analysis method of Lévy series expansion, detailed for the first time

in this manuscript for a positive definite function, may find several important applications in the future, in a broad range of quantitative sciences. Essentially this method is able to characterize the deviations from Fourier-transformed and symmetric Lévy stable source distributions. Given the ubiquity of Lévy distributions in Nature, we hope that our new method will be relevant in several areas of human knowledge, that extend far beyond the science of physics.

Acknowledgments

We gratefully acknowledge inspiring physics discussions with professors W. Guryn, G. Gustafson, L. Lönnblad, and M. Šumbera. T.Cs. and A.S. thank the Lund university for kind hospitality and support during their visit. T.Cs. would like to thank to Prof. R.J. Glauber for inspiring discussions and for proposing a series expansion to describe the forward scattering amplitude. We are thankful to the TOTEM Collaboration at CERN LHC, in particular, to S. Giani, the Spokesperson, and K. Osterberg, the Physics Coordinator, for making the TOTEM preliminary 13 TeV data set available for us. R.P. is partially supported by the Swedish Research Council, contract numbers 621-2013-4287 and 2016-05996, by CONICYT grants PIA ACT1406 and MEC80170112, as well as by the European Research Council (ERC) under the European Union's Horizon 2020 research and innovation programme (grant agreement No 668679). The work has been performed in the framework of COST Action CA15213 "Theory of hot matter and relativistic heavy-ion collisions" (THOR). Our research was partially supported by the Hungarian NKIFH grants No. FK-123842 and FK-123959, the Hungarian EFOP 3.6.1-16-2016-00001 project and the exchange programme of the Hungarian and the Ukrainian Academies of Sciences, grant NKM-92/2017.

A Lévy expansion fits to elastic *pp* collisions: full acceptance region

In this Appendix, we describe the results of the fourth-order Lévy expansion fits to the elastic scattering data of *pp* collisions for five different data sets, measured in the ISR energy range of $\sqrt{s} = 23.5$, 30.7, 44.7, 52.8 and 62.5 GeV. The parameters of the fourth-order Lévy expansion are shown on the corresponding figures, together with the extracted value of the total cross-section, the value of the ρ parameter and the measures of the fit quality.

Many of the features of these fit results are common for all of these plots, but let us start with noting that the fits, although look quite reasonable to the naked eye, differ in their quality. The confidence level of fits to the $\sqrt{s} = 23.5$, 30.7 and 62.5 GeV data sets has a statistically acceptable value, with CL > 0.1 %, while the quality of the fits to the data sets at $\sqrt{s} = 44.7$ and 52.8 GeV is not acceptable from the point of the mathematical statistics, corresponding to CL $\ll 0.1$ % . This implies that we are not allowed to interpret the results of the fits to the 44.7 and 52.8 GeV data sets, as the fitted curve, although looks reasonable, does not represent the data well enough (from the mathematical statistics point of view).

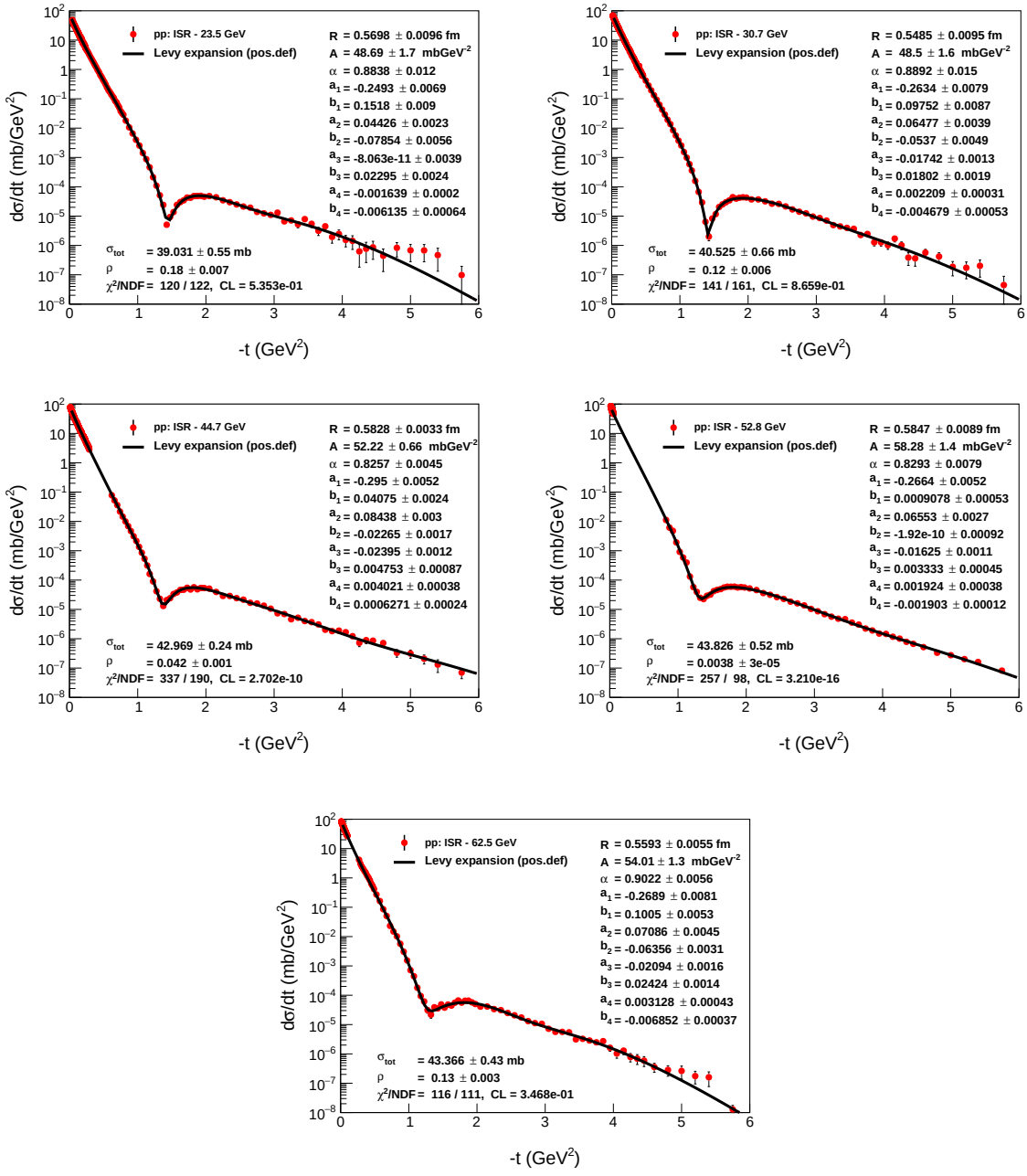


Figure 18. Fourth-order Lévy expansion fits of the differential cross-section data from Ref. [45] on pp elastic scattering at $\sqrt{s} = 23.5$ GeV (upper left), $\sqrt{s} = 30.7$ GeV (upper right), $\sqrt{s} = 44.7$ GeV (middle left), $\sqrt{s} = 52.8$ GeV (middle right), $\sqrt{s} = 62.5$ GeV (bottom).

B Lévy expansion fits to elastic $p\bar{p}$ collisions: full acceptance region

In this Appendix, we describe the third-order Lévy expansion fits to the elastic scattering data of $p\bar{p}$ collisions for four different data-sets, at $\sqrt{s} = 53$, 546, 630 and 1960 GeV.

Some of the features are common for all of these plots.

1) The parameters $\alpha = 0.9$ and $R = 0.65$ fm were found to be within the errors independent of $\sqrt{s}$, so they were fixed to a collision energy independent constant value in these cases. It is an interesting and open problem to search for a physics interpretation of the universality of the α and R values of elastic $p\bar{p}$ collisions, but this topic goes beyond the scope of the model-independent approach followed in the current manuscript. As an extra bonus, fixing these $\alpha = 0.9$ and $R = 0.65$ fm parameter values has resulted in a reasonably good reproduction of the $\sqrt{s}$ dependence of the total $p\bar{p}$ cross-sections, achieved without an additional tuning.

2) These $p\bar{p}$ elastic scattering data were less detailed as compared to the corresponding $p\bar{p}$ data, presented in Appendix A. The "dip" region was covered in all the cases, however, at very low $|t|$ as well as at large $|t|$ values, the acceptance and thus the t range were rather limited. This prevented us from a reliable analysis of the ρ parameter of elastic scattering for these collisions even at $t = 0$.

3) We have tested if the third-order and fourth-order Lévy expansions give similar results for these data sets or not. Within errors, the fourth-order expansion parameters were found to be consistent with zero, so we have fixed them to zero and investigated the third-order Lévy expansion results.

4) We have checked that $\rho(t = 0)$ changes well outside the Minuit indicated errors, if we change the order of the expansion from a third-order to a fourth-order Lévy expansion. Usually high precision data at low values of $|t|$ are needed to reconstruct ρ reliably, so this limitation is not unexpected. However, it indicates the sensitivity of our method. In contrast to $\rho(t)$, the $B(t)$ slope parameters and the $P(b)$ shadow profiles were found to be stable with respect to increasing the order of the Lévy expansion from the third to the fourth order.

5) We have found that a third-order Lévy expansion provides a reasonable overall description for all of these four data sets: Minuit has converged, error matrix accurate, and the fit quality is not unacceptable. The confidence level is sufficiently large, CL > 0.1 % for all the four data sets. We concluded, that with the exception of the overly sensitive parameter ρ, we can interpret the physical meaning of the fit parameters, as they represent the data. Note that the $|t|$ ranges of the various data sets are rather different, but it is clear that the Lévy expansion reproduces the elastic $p\bar{p}$ differential cross-section in the respective s and $|t|$ ranges of these four data-sets.

The parameters of the third-order Lévy expansion are shown on the corresponding figures, together with the extracted values of the total cross-section, and the measures of the fit quality. The value of the ρ parameter is also shown, but the fluctuation of these values as a function of $\sqrt{s}$ also indicates that even the value of $\rho(t = 0)$ cannot be reliably determined from the these $p\bar{p}$ elastic scattering data.

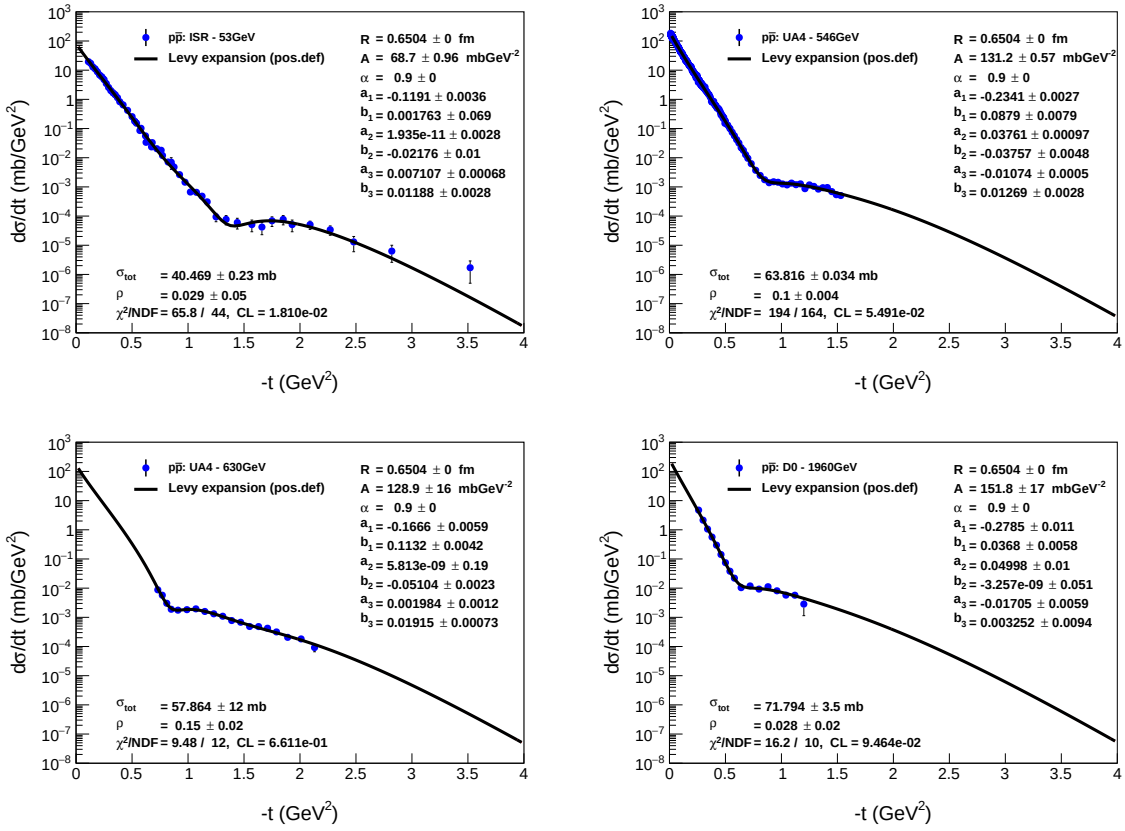


Figure 19. Third-order Lévy expansion fits of the differential cross-section data on $p\bar{p}$ elastic scattering at $\sqrt{s} = 53$ GeV [46] (upper left), $\sqrt{s} = 546$ GeV [47] (upper right), $\sqrt{s} = 630$ GeV (bottom left) [48], $\sqrt{s} = 1960$ GeV [50] (bottom right), with fixed $\alpha = 0.9$ and $R = 0.65$ fm.

C Lévy fits to elastic pp collisions at large $|t|$

In this Appendix, we detail the Lévy fits, $d\sigma/dt = A \exp\left(-(R^2 t)^\alpha\right)$ to the elastic scattering data of pp collisions for seven different data sets, at $\sqrt{s} = 23.5$, 30.7, 44.7, 52.8, 62.5 GeV as well as at 7 and 13 TeV. These fits correspond to the zeroth order, leading terms of the Lévy expansions, with all the expansion coefficients set to zero or $c_i = 0$, as detailed in Subsection 2.1.

Some of the features are common for all of these plots.

In the ISR energy domain fits were performed in the $2.5 < |t| < 5$ GeV^2 region. In each case, Minuit has converged, error matrix was accurate, and the confidence level of the fits was acceptable, with CL > 0.1 %. In each case, the value of the parameter α was, within errors, consistent with 0.9 so we have fixed its value to 0.9 in each case. Let us note, however, that the fixed value of this parameter α can be varied between 1.0 and 0.8 without changing the acceptability of the fit, so the criteria of CL > 0.1 % was satisfied.

The good quality of these fit results indicates, that a substructure is present inside the protons: the data after the dip and bump region have the same structure and quality, as a usual low-$|t|$ elastic scattering data below the dip region, used to be parametrized by a nearly exponential shape. However, the related cross-sections and length-scales are smaller than that of the protons. This conclusion is rather obvious after one compares the results of the Lévy fits to the tail or large-$|t|$ regions, as presented in Appendix C with the results of Lévy fit results in the cone or low-$|t|$ region, as detailed in Appendix D below. These comparisons were summarized clearly in Fig. 6 for the tail and in Fig. 7 for the cone region. It is quite remarkable, that the proton substructure in the ISR region has a size that is apparently independent of the change of the energy in the region of a few tens of GeV, but this substructure appears to be different (in size) from a substructure that is emerged in pp collisions in the 7 – 13 TeV energy range, as evidenced from the parallel dashed lines in Fig. 6.

We have also studied the stability of these fits. Increasing the value of α decreased the Lévy scale R and the contribution to the total cross-section. Taking into account a co-variation of the fit parameters with the fixed value of α we find that in each of these data sets, we are allowed to vary the value of α in a reasonable range of 0.8 to 1.0. We found that in each case the same-size substructure of the proton was present, with a characteristic Lévy length scale of $R_{\rm ISR} = 0.3 \pm 0.1$ fm, and a contribution to the total cross-section with $\sigma_{\rm ISR} = 0.3^{+0.3}_{-0.1}$ mb, where the quoted errors take into account the errors coming from a variation of the value of α as well. Apparently, the same structure is seen in these reactions, within the systematic error of the analysis, as indicated in Fig. 20.

However, the same type of analysis reveals a different-size proton substructure, when one performs a similar analysis in the TeV energy range. Fits to the differential cross-sections of elastic pp scattering data at $\sqrt{s} = 7$ TeV and preliminary TOTEM data at $\sqrt{s} = 13$ TeV are shown in Fig. 20 in the lower middle right and bottom panels, respectively. This substructure corresponds to a Lévy scale of $R_{\rm LHC} = 0.5 \pm 0.1$ fm, and to a contribution to the total cross-section with $\sigma_{\rm LHC}(13\ {\rm TeV}) = 6.1^{+3.3}_{-2.6}$ mb at 7 TeV, which is within the errors the same as the preliminary value of $\sigma_{\rm LHC}(13\ {\rm TeV}) = 10.2^{+5.9}_{-4.7}$ mb at 13 TeV. It is clear that these scales of R and the contributions to the total cross-section at the level of $\sigma_{\rm LHC} \approx 8.2^{+7.9}_{-4.7}$ mb, that emerge at the TeV scale colliding energies, are significantly larger than the corresponding cross-sections and scales in the ISR energy range of 23.5 – 62 GeV. The errors of $R_{\rm LHC}$ and $\sigma_{\rm LHC}$ include the estimated systematic uncertainties as well, and those are larger than the statistical errors shown on the figures. Indeed, they also take into account the fact, that similar results were obtained for $\alpha = 0.8$ and $\alpha = 1.0$ fixed values as well, where the increasing or decreasing of α value has resulted in a decrease or increase of R (and σ), respectively.

The emergence of the proton substructure with two different sizes in elastic pp collisions at the ISR energy range of $\sqrt{s} = 23.5$ – 62.5 GeV and at the LHC energy range of $\sqrt{s} = 7$ – 13 TeV, respectively, is clearly demonstrated on the summary plot that shows the data and the Lévy fit results to the tails of the differential cross-sections of elastic pp collisions on the same plot, also indicating with dashed lines the extrapolation of the fit results outside the

fitted domain, see Fig. 6.

The change of the slope of these lines from ISR to the LHC energies is so much obvious and striking to the naked eye, that it is rather surprising that such a change was not reported in the literature before, at least, to the best of our knowledge. Perhaps, the reason for this effect is the expectation, that perturbative QCD effects should start to be visible soon after the dip-bump structure which could result in a power-law decrease of the differential elastic cross-section. Indeed, such a power-law fit was performed and published by the TOTEM Collaboration in Ref. [49] when analysing the first set of 7 TeV elastic scattering data. In particular, the TOTEM Collaboration has reported that for $|t|$-values larger than $\sim$1.5 GeV^2, the differential cross-section of elastic pp collisions exhibits a power law behaviour, with an exponent of -7.8 ± 0.3 (stat) ± 0.1 (syst).

Given that the new (but still preliminary) TOTEM data at 13 TeV are much more detailed and cover an extended $|t|$ range after the dip and bump structure, we can easily test the presence (or not) of the perturbative QCD predicted power-law tails in these elastic scattering data: if $d\sigma/dt \propto |t|^n$ then the power-law tail emerges as a straight line on a log-log plot.

In order to illustrate this point, we have prepared such a log-log plot that includes the TOTEM preliminary $d\sigma/dt$ data at $\sqrt{s} = 13$ TeV, and the Lévy expansion fit results. As clearly seen in Fig. 14, the tail is not a straight line on this plot, so the $|t|$-range is apparently not yet in the domain of perturbative QCD, with a possible exception for data points close to the end of the acceptance region at large $|t|$ (within rather big error bars though).

D Lévy fits to elastic pp collisions at small $|t|$

In this Appendix, we describe the zeroth-order Lévy fits, $d\sigma/dt = A \exp\left(-(R^2 t)^\alpha\right)$ to the low-$|t|$ or cone region of elastic pp scattering data for seven different data sets, at $\sqrt{s} = 23.5$, 30.7, 44.7, 52.8, 62.5 GeV as well as at 7 and 13 TeV.

Traditionally, an exponential behaviour is assumed for this kinematic region, with $\alpha = 1$ fixed fits. However, recently the TOTEM collaboration demonstrated a non-exponential behaviour in $\sqrt{s} = 8$ TeV pp collisions, that was found to be significant, corresponding to a more than 7σ effect [25]. These results were highlighted and some of their implications and ramifications were detailed also in Ref. [51]. In this Appendix, we re-examine the other, already published data sets using the zeroth-order Lévy fits, where the selected low-$|t|$ regions are very similar to the 8 TeV analysis of TOTEM, namely we fit a $|t|$ region that is similar to the TOTEM analysis at 8 TeV, when $|t|$ is measured in units of $t_{\rm dip}$. Our fit region is thus $0.04\,|t|_{\rm dip} \le |t| \le 0.4\,|t_{\rm dip}|$. We have performed a detailed investigation of this region and found that all the data sets were described with a good confidence level with the zeroth-order Lévy fit, with only three free parameters, A, R and α. Within the errors, in the ISR region, the values of the parameter α were in the region of 0.90 ± 0.02 in these fits. Hence, we have fixed the value of α to 0.9, that allowed us to demonstrate the trends more clearly and also to compare the results with the similar analysis in the large $|t|$ region.

All the data in the ISR energy range were fitted successfully with a CL ≥ 0.1 % for the $\alpha = 0.9$ fixed case as well. The Lévy radii R kept on increasing monotonically with increasing $\sqrt{s}$. The best fit parameters as well as the fit quality measures are indicated in Fig. 21.

However, the fixed $\alpha = 0.9$ fits failed both on the $\sqrt{s} = 7$ TeV final and on the $\sqrt{s} = 13$ TeV preliminary data. These fit results, although on a qualitative level apparently may be called as "satisfactory", are statistically not acceptable. This implies that in the TeV energy region, some new mechanism starts to work, that changes not only the Lévy scale but also the shape of the proton. Actually, from the analysis of the shadow profile function, we know that such a new effect in the TeV energy range corresponds to the saturation of the shadow profile functions $P(b)$ in the region of $b \leq 0.4 - 0.5$ fm. This result, detailed in Subsection 3.2 is supported strongly and independently by the fits detailed above.

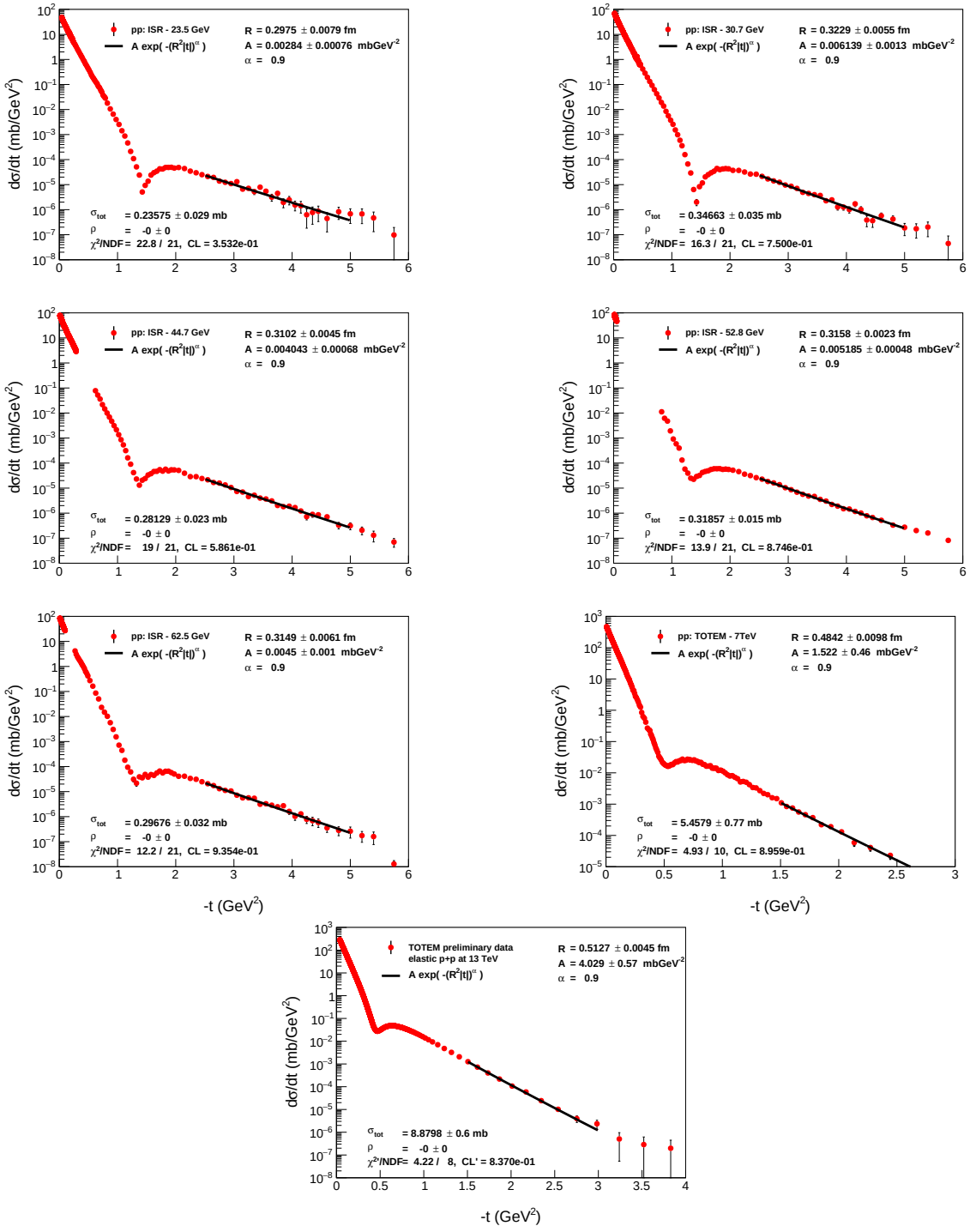


Figure 20. Zeroth-order Lévy fits to the tail of the differential cross-section data on pp elastic scattering at $\sqrt{s} = 23.5$ GeV [45] (upper left), $\sqrt{s} = 30.7$ GeV [45] (upper right), $\sqrt{s} = 44.7$ GeV [45] (upper middle left), $\sqrt{s} = 52.8$ GeV [45] (upper middle right), $\sqrt{s} = 62.5$ GeV [45] (lower middle left), $\sqrt{s} = 7$ TeV (lower middle right), TOTEM preliminary $\sqrt{s} = 13$ TeV (bottom), with fixed $\alpha = 0.9$, A and R as free fit parameters.

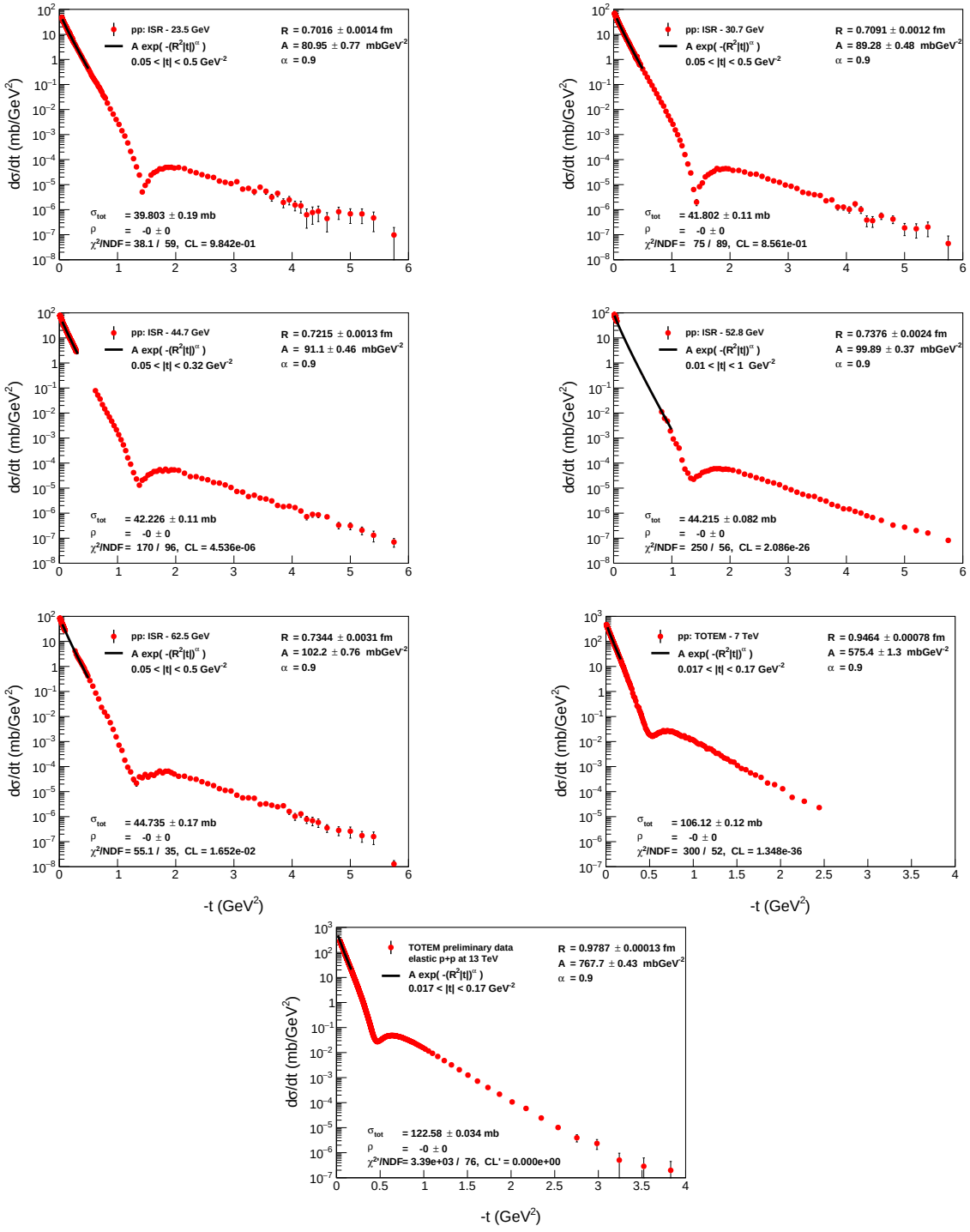


Figure 21. Zeroth-order Lévy fits to the cone region of the differential cross-section data on pp elastic scattering at $\sqrt{s} = 23.5$ GeV [45] (upper left), $\sqrt{s} = 30.7$ GeV [45] (upper right), $\sqrt{s} = 44.7$ GeV [45] (upper middle left), $\sqrt{s} = 52.8$ GeV [45] (upper middle right), $\sqrt{s} = 62.5$ GeV [45] (lower middle left), $\sqrt{s} = 7$ TeV (lower middle right), TOTEM preliminary $\sqrt{s} = 13$ TeV (bottom), with fixed $\alpha = 0.9$, A and R being free fit parameters.

References

[1] G. Antchev *et al.* [TOTEM Collaboration], arXiv:1712.06153 [hep-ex], Preprint CERN-EP-2017-321, http://cds.cern.ch/record/2298154.

[2] G. Antchev *et al.* [TOTEM Collaboration], Preprint CERN-EP-2017-335, http://cds.cern.ch/record/2298154.

[3] L. Lukaszuk and B. Nicolescu, Lett. Nuovo Cim. **8**, 405 (1973).

[4] A. Ster, L. Jenkovszky and T. Csörgő, Phys. Rev. D **91**, no. 7, 074018 (2015) [arXiv:1501.03860 [hep-ph]].

[5] A. P. Samokhin and V. A. Petrov, Nucl. Phys. A **974**, 45 (2018) [arXiv:1708.02879 [hep-ph]].

[6] V. A. Khoze, A. D. Martin and M. G. Ryskin, Phys. Rev. D **97**, no. 3, 034019 (2018) [arXiv:1712.00325 [hep-ph]].

[7] V. A. Petrov, Eur. Phys. J. C **78**, no. 3, 221 (2018) Erratum: [Eur. Phys. J. C **78**, no. 5, 414 (2018)] [arXiv:1801.01815 [hep-ph]].

[8] V. A. Khoze, A. D. Martin and M. G. Ryskin, Phys. Lett. B **780**, 352 (2018) [arXiv:1801.07065 [hep-ph]].

[9] V. P. Gonçalves and B. D. Moreira, Phys. Rev. D **97**, no. 9, 094009 (2018) [arXiv:1801.10501 [hep-ph]].

[10] Y. M. Shabelski and A. G. Shuvaev, Eur. Phys. J. C **78**, no. 6, 497 (2018) [arXiv:1802.02812 [hep-ph]].

[11] M. Broilo, E. G. S. Luna and M. J. Menon, arXiv:1803.06560 [hep-ph].

[12] M. Broilo, E. G. S. Luna and M. J. Menon, Phys. Lett. B **781**, 616 (2018) [arXiv:1803.07167 [hep-ph]].

[13] P. Lebiedowicz, O. Nachtmann and A. Szczurek, arXiv:1804.04706 [hep-ph].

[14] E. Martynov and B. Nicolescu, arXiv:1804.10139 [hep-ph].

[15] S. M. Troshin and N. E. Tyurin, arXiv:1805.05161 [hep-ph].

[16] I. M. Dremin, Universe **4**, no. 5, 65 (2018).

[17] W. Broniowski, L. Jenkovszky, E. Ruiz Arriola and I. Szanyi, arXiv:1806.04756 [hep-ph].

[18] V. A. Khoze, A. D. Martin and M. G. Ryskin, arXiv:1806.05970 [hep-ph].

[19] F. Nemes for the TOTEM Collaboration, Proc. of the 4th Elba workshop on Forward Physics @ LHC energy, 24-26 May 2018, Elba, Italy, in preparation, to be published in a special issue of Instruments; https://indico.cern.ch/event/705748/
Fabio Ravera for the TOTEM collaboration, 134th LHCC meeting - open session, 30 May 2018; https://indico.cern.ch/event/726320/ .

[20] T. Csörgő and S. Hegyi, Phys. Lett. B **489** (2000) 15.

[21] M. B. De Kock, H. C. Eggers and T. Csörgő, PoS WPCF **2011** (2011) 033.

[22] A. Adare *et al.* [PHENIX Collaboration], Phys. Rev. C **97**, no. 6, 064911 (2018) [arXiv:1709.05649 [nucl-ex]].

[23] T. Novák, T. Csörgő, H. C. Eggers and M. de Kock, Acta Phys. Polon. Supp. **9**, 289 (2016) [arXiv:1604.05513 [physics.data-an]].

[24] M. M. Block, Phys. Rept. **436**, 71 (2006) [hep-ph/0606215].

[25] G. Antchev *et al.* [TOTEM Collaboration], Nucl. Phys. B **899**, 527 (2015) [arXiv:1503.08111 [hep-ex]].

[26] C. Tsallis, S. V. F. Lévy, A. M. C. Souza and R. Maynard, Phys. Rev. Lett. **75**, 3589 (1995).

[27] E. W. Weisstein, "Stable Distribution." From MathWorld–A Wolfram Web Resource. http://mathworld.wolfram.com/StableDistribution.html

[28] J. P. Nolan, *Stable distributions: Models for Heavy Tailed Data*, Springer-Verlag, Imprint Birkhauser, ISBN10 0817641599, (2016), pp. 1-352.

[29] A. Ster et al, *Model independent analysis of data with nearly Gaussian or Lévy shape*, proceedings of the 10th Bolyai-Gauss-Lobachevsky conference BGL17, Gyöngyös, Hungary, August 20-26, 2017, https://indico.cern.ch/event/586799/contributions/2695964/

[30] T. Novák et al, *Model independent analysis of nearly Lévy sources*, proceedings of the 12th Workshop on Particle Correlations and Femtoscopy, Cracow, Poland, May 22-26, 2018, https://indico.ifj.edu.pl/event/199/contributions/1166/

[31] T. Csörgő, S. Hegyi and W. A. Zajc, Eur. Phys. J. C **36** (2004) 67.

[32] G. Antchev *et al.* [TOTEM Collaboration], EPL **101**, no. 2, 21002 (2013).

[33] L. L. Jenkovszky, A. I. Lengyel and D. I. Lontkovskyi, Int. J. Mod. Phys. A **26**, 4755 (2011) [arXiv:1105.1202 [hep-ph]].

[34] R. J. N. Phillips and V. D. Barger, Phys. Lett. **46B**, 412 (1973).

[35] F. Nemes, T. Csörgő and M. Csanád, Int. J. Mod. Phys. A **30**, no. 14, 1550076 (2015) [arXiv:1505.01415 [hep-ph]].

[36] A. K. Kohara, E. Ferreira and T. Kodama, Eur. Phys. J. C **74**, 3175 (2014) [arXiv:1408.1599 [hep-ph]].

[37] P. Lipari and M. Lusignoli, Eur. Phys. J. C **73**, no. 11, 2630 (2013) [arXiv:1305.7216 [hep-ph]].

[38] I. M. Dremin, EPJ Web Conf. **145**, 10003 (2017).

[39] M. Csanád, T. Csörgő, Z. F. Jiang and C. B. Yang, Universe **3**, no. 1, 9 (2017) [arXiv:1609.07176 [hep-ph]].

[40] B. Z. Kopeliovich, I. K. Potashnikova, B. Povh and E. Predazzi, Phys. Rev. Lett. **85**, 507 (2000) [hep-ph/0002241].

[41] B. Z. Kopeliovich, I. K. Potashnikova, B. Povh and E. Predazzi, Phys. Rev. D **63**, 054001 (2001) [hep-ph/0009008].

[42] B. Z. Kopeliovich, I. K. Potashnikova and B. Povh, Phys. Rev. D **86**, 051502 (2012) [arXiv:1208.5446 [hep-ph]].

[43] N. A. Amos *et al.* [E710 Collaboration], Phys. Rev. Lett. **68**, 2433 (1992).

[44] S. J. Brodsky, Adv. High Energy Phys. **2018**, 7236382 (2018) [arXiv:1709.01191 [hep-ph]].

[45] U. Amaldi and K. R. Schubert, Nucl. Phys. B **166**, 301 (1980).

[46] A. Breakstone *et al.* [AMES-BOLOGNA-CERN-DORTMUND-HEIDELBERG-WARSAW Collaboration], Nucl. Phys. B **248**, 253 (1984).

[47] D. Bernard *et al.* [UA4 Collaboration], Phys. Lett. B **198**, 583 (1987).

[48] D. Bernard *et al.* [UA4 Collaboration], Phys. Lett. B **171**, 142 (1986).

[49] G. Antchev *et al.* [TOTEM Collaboration], EPL **95**, no. 4, 41001 (2011) [arXiv:1110.1385 [hep-ex]].

[50] V. M. Abazov *et al.* [D0 Collaboration], Phys. Rev. D **86**, 012009 (2012) [arXiv:1206.0687 [hep-ex]].

[51] T. Csörgő [TOTEM Collaboration], EPJ Web Conf. **120**, 02004 (2016) [arXiv:1602.00219 [hep-ex]].